Use of Electrical Resistance Heating and Electrical Heater Heating to Remove Condensate Blockage in the Near-wellbore Region

by
Siyuan Wang

A thesis submitted in partial fulfillment of the requirements for the degree of

Master of Science
in
Petroleum Engineering

Department of Civil and Environmental Engineering

University of Alberta

Abstract

During the production of gas condensate from a reservoir, a gas condensate bank may be formed in the near-wellbore region, leading to reduced long-term productivity. The major existing remedial methods for removing the condensate bank include cyclic gas injection, solvent injection, wettability alternation using surfactants, etc. The drawbacks of the existing methods are that their nature of requiring injecting fluid into formation limits their application in low-permeability formations, and their field execution may disturb the normal production of gas condensate. The presented approach uses an electrical heater, or an electrode installed at the bottomhole to remove the condensate bank, avoiding injecting fluid into the reservoir and eliminating the need for workover operations when executing the remedial job. We carry out numerical simulation studies to examine the feasibility of the new approach.

A conceptual reservoir model was built with an appropriate simulator CMG STARS. Simulation results show that the approach provides good production restoration in low permeability reservoirs with condensate blockage issues. By heating the near-wellbore region, the operation increases both temperature and pressure around the wellbore. Such increases, on one hand, lead to shifting of the phase envelope, which results in re-vaporization of the condensate bank; on the other hand, the increases in temperature and pressure reduce the capillary force, decreasing the residual oil saturation and mobilizing condensate that cannot be recovered at the original pressure and temperature conditions. In conclusion, the study provides an alternative solution to the remediation of condensate blockage that is easy to set up and convenient to control. Compared with other methods, the new approach requires only one operation to install the heating element and offers a long-term remedy for production loss caused by the condensate bank.

Dedication

To my loving Mom and Dad.

Acknowledgements

I would like to express my sincere thanks to my supervisor, Dr. Huazhou (Andy) Li, for his continuous guidance and support during my master's program. I would also thank my examination committee chair, Dr. Ergun Kuru, and my examination committee members, Dr. Hongbo Zeng and Dr. Juliana Leung for their critical and valuable comments and suggestions. In addition, I want to thank Dr. Moran Wang, Mr. Yihang Wang, and Mr. Guang Yang from Tsinghua University for their willingness to impart knowledge and provide help. Moreover, I want to thank my family who gives me financial and spiritual support. Finally, as a part of the University of Alberta's Future Energy Systems research initiative, this research was made possible in part thanks to funding from the Canada First Research Excellence Fund.

Table of Contents

List of Tables

List of Figures

Chapter 1 Introduction

1.1 Research Background

Gas condensate reservoir takes up a notably large amount of low-permeability unconventional reserves (Orangi et al., 2011). However, condensate build-up and blockage constantly hinders the economical development of unconventional condensate reservoirs. Liquid-rich tight/shale gas condensate is considered as one of the most profitable and environment-friendly unconventional hydrocarbon resources. It yields a significant amount of valuable condensate which has extensive applications, such as serving as a high-quality crude or diluting bitumen for transportation through pipelines (Rahimi et al., 2009).

As shown in **Figure 1**, gas condensate refers to reservoir fluids whose in-situ reservoir temperature is greater than the critical temperature but less than the cricondentherm (Whitson et al., 2000). The liquid content in a gas condensate reservoir increases counterintuitively when the pressure around the wellbore drops below the dew point as a result of continuous production. The phenomenon was firstly described by Kuenen (1892) with the term "retrograde condensation". This unique feature of gas condensate causes extra difficulties in its production. When hydrocarbons are depleted from a gas condensate reservoir, pressure around the production wellbore decreases rapidly. Once the near-wellbore pressure reaches the dew point pressure, a condensate bank starts to build around the wellbore. The existence of the condensate bank will block the original flow paths of the gaseous phase and transform the flow regime into a 2-phase flow (herein assuming there is no connate water). As the bottomhole flowing pressure continues to draw down, the condensate bank expands and further reduces the well productivity.

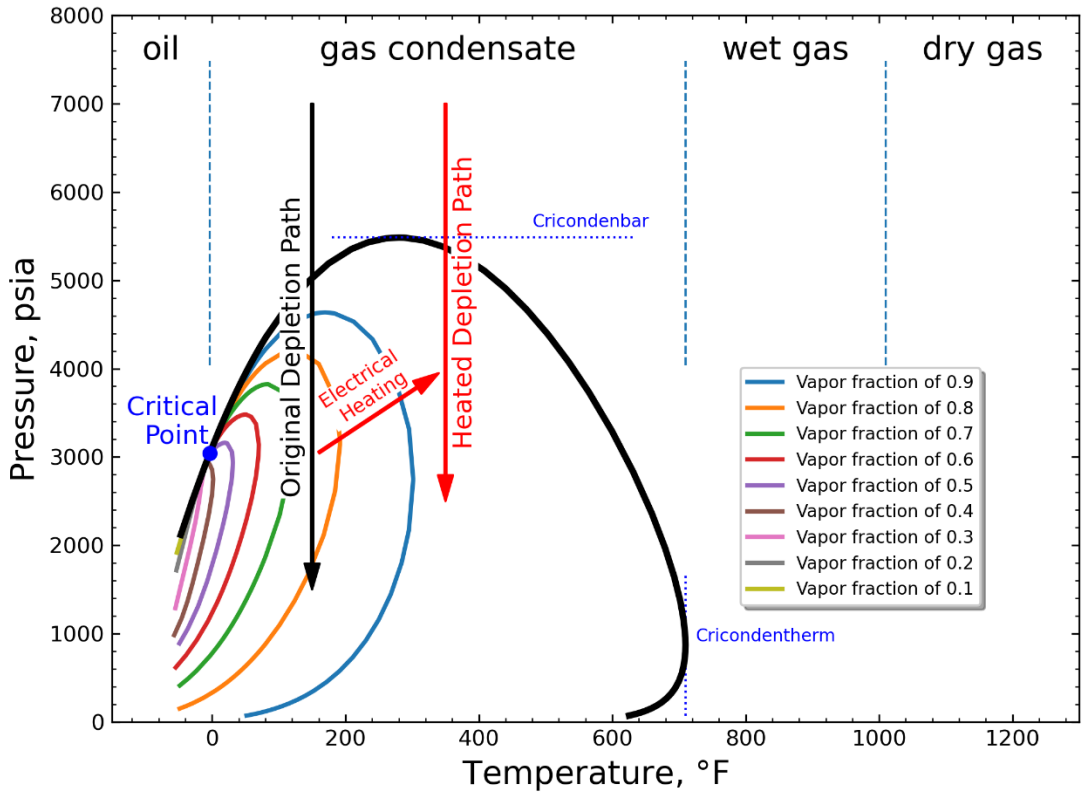

Figure 1. Schematic showing the classification of the reservoir fluid and the effect of heating on the depletion path of a gas condensate reservoir.

The liquid dropout due to retrograde condensation will block the flow path of the gaseous phase, causing a reduction of the relative permeability of the gaseous phase. The flow path blockage effect aggravates with a decreasing formation permeability. When the formation permeability is low enough, there exists some saturation range where the effective permeability of both phases is too small to have a practically measurable flow of both phases. This behaviour in a gas and water system is described as the "Permeability Jail" phenomenon by Shanley et al. (2004). Byrnes & Cluff (2010) provided a quantitative definition of such phenomenon, claiming that the porous material is in a permeability jail when the saturation is in a certain range where the relative permeability of both gaseous and aqueous phase is smaller than 2%. The saturation range usually

falls between 55-80% water saturation. We believe that such phenomenon applies to condensate blockage as well, but with a weaker permeability hindrance effect since the capillary force between gas and condensate is smaller than that between gas and water.

1.2 Existing Efforts

Several remedial efforts have been proposed and tested to mitigate the productivity losses caused by the condensate bank in both conventional and low permeability formations. These efforts include the injection of solvents, gas cycling/injection, wettability alteration, etc (Sayed & Al-Muntasheri, 2016). Some methods may be more effective than the others in a certain formation, but all of the efforts use one or more of the following mechanisms: (1) maintaining or restoring a pressure in the reservoir greater than the dew point pressure; (2) decreasing the capillary force that prohibits the gas phase from flowing; and (3) changing reservoir fluid composition around the wellbore to manipulate its PVT behaviours. The solvent injection method injects low molecule-weight solvents, most likely alcohols (such as methanol, ethanol, and isopropanol) into the reservoir to improve the gas relative permeability (Du et al., 2000). The solvent is partially miscible with both oleic and aqueous phases at reservoir conditions, resulting in a miscible displacement of water and condensate (Du et al., 2000). The results of the treatment are two-fold: (1) removal of the condensate blockage, which could recur in the future due to continuous pressure drawdown and condensate buildup; and (2) removal of water that could potentially last longer (Al-Anazi et al., 2002). The gas injection method injects produced dry gas, nitrogen, or carbon dioxide into the reservoir to maintain the reservoir pressure, reducing the dew point pressure of reservoir gas by changing its composition (Sayed & Al-Muntasheri, 2016). The method can be operated with either a huff-n-puff mode or a gas-flooding mode. The wettability alteration method involves using fluorinated surfactants and fluorinated polymers to change the wettability of the reservoir rock

from water-wet or oil-wet to more favourable intermediate wetting or, sometimes, gas wetting (Sayed & Al-Muntasheri, 2016). The change in wettability leads to the reduction of capillary force, which facilitates the displacement of water and condensate by gas. After all, the wettability alteration treatment reduces the residual oil saturation and restores the gas relative permeability (Kumar et al., 2006). **Table 1** summarizes the advantages and disadvantages of the remedial operations that have been implemented to resolve the condensate banking issue.

Table 1. Pros and cons of the existing remedial operation for condensate banking (Aziz, 1983; Du et al., 2000; Kumar et al., 2006; Sayed & Al-Muntasheri, 2016)

Remedial operations	Pros	Cons
Solvent injection	• The method relieves water banking as well. • It is theoretically possible to achieve 100% liquid recovery by this method.	• The injection is hindered by low permeability. • It requires frequent pause of the normal production to implement the injection. • The solvent is usually costly.
Wettability alteration	• The effect usually lasts longer than other operations. • The method relieves water banking as well.	• The injection is hindered by low permeability. • An incautious operation may cause permanent damage to the reservoir.
Gas injection (cycling and flooding)	• It is possible to completely prevent the condensation if the reservoir pressure is maintained above the dew point.	• The injection is hindered by low permeability. • It requires frequent pause of the normal production to implement the injection for the cycling mode.
Drill horizontal well, hydraulic fracturing, acidizing, and other well productivity improvement methods.	• A production increase is usually guaranteed. • The method can be combined with other operations.	• The method does not resolve the condensation issue directly. • The operation is usually costly.

1.3 Problem statement

Most of the traditional remedial methods mentioned previously involve injecting fluids into the reservoir, and some of them require on-site treatment periodically. These features give rise to some problems, especially when implemented in low permeability formations. Firstly, the limited injectivity in low permeability formation impedes the successful implementation of conventional remedial methods. It takes a longer time for the fluid to reach enough penetration depth and to come into effect. Secondly, some of the treatments interrupt the normal production of the reservoir, causing a higher opportunity cost of the remedial methods. Together with the extended operation time due to low injectivity, the production interruption further impairs the economic feasibility of the traditional remedial methods. Thirdly, some conventional remedial methods only delay condensate blockage from happening but never resolve the issue from the fundamentals. The production improvement could only last for a short period. Condensate will accumulate around the wellbore again shortly after the treatment. The production improvement period shall be even shorter in low permeability formations than that in conventional reservoirs due to a more severe pressure drop.

1.4 Research Objectives

Due to the limits of the existing remedial methods, there is enough motivation for us to design a new operational method to resolve the condensate blockage issue effectively in a low-permeability formation with long-lasting performance and reasonable cost. Alafnan et al. (2019) proposed an enhanced recovery method from condensate reservoirs by heating, but the heat and mass transfer in the reservoir and the economic feasibility of the method are not studied in detail. In this research, we apply heat to the reservoir to remove the condensate bank in the near-wellbore region in low-permeability shale/tight sandstone formations. By heating the near-wellbore region, we introduce

energy to the formation region where the condensate banking issue is most serious. The heating will increase both temperature and pressure. The change in temperature and pressure converts a fraction of, or in rare cases, all of the liquid condensate to a gaseous phase whose viscosity is significantly lower (See **Figure 1**). Moreover, the heating reduces the capillary force; and most importantly, the phase change leads to an increase in gas saturation, which further results in an increase in gas relative permeability.

Different heating systems could be implemented to alleviate the condensate build-up around the wellbore, enhancing the production of a gas condensate well. In this research, we propose to apply the heating with the downhole electrical heater heating (DHEH) or electrical resistance heating (ERH). Reasons for choosing such a heating system include the following: 1) the system requires a less up-front investment; 2) the process can be easily monitored and controlled; 3) and the system has an acceptable efficiency. The former method is realized by an electrical line heater embedded in the cement around the casing. The heat is transferred into the reservoir through conduction. Whereas the latter is accomplished with an electrode with low-frequency electricity supplied to it. The potential difference between the electrode and the formation causes current to pass through the reservoir. Heat is generated by the Joule effect. Electricity is transmitted to the bottomehole through power cables running in the casing-tubing annulus for both methods. Several energy resources including renewable energy such as solar power could be used to generate the required electricity, further promoting the energy efficiency of the method (Alafnan et al., 2019).

This paper will conduct simulation studies to investigate the performance and feasibility of the proposed methods. The simulation studies involve two parts: firstly, a Peng-Robinson Equation of State (PR-EOS) (Peng & Robinson, 1976) is used to capture the pressure, volume, and temperature (PVT) behaviour of a representative gas condensate fluid; secondly, a reservoir-scale numerical

simulation was conducted with an appropriate reservoir model and the established fluid model to evaluate the heat propagation in the near-wellbore region and to estimate the overall performance of the operation. Lastly, the economic feasibility of the method is studied with the net present value (NPV) analysis and energy return on investment (EROI) analysis.

References

Alafnan, S., Aljawad, M., Alismail, F., & Almajed, A. (2019). Enhanced Recovery from Gas Condensate Reservoirs through Renewable Energy Sources. Energy and Fuels, 33(10), 10115–10122.

Al-Anazi, H. A., Pope, G. A., Sharma, M. M., & Metcalfe, R. S. (2002). Laboratory Measurements of Condensate Blocking and Treatment for Both Low and High Permeability Rocks. SPE 77546.

Aziz, R. M. (1983). A 1982 Critique on Gas Cycling Operations on Gas-Condensate Reservoirs. SPE 11477.

Cluff, R. M., & Byrnes, A. P. (2010). Relative Permeability in Tight Gas Sandstone Reservoirs - the "Permeability Jail" Model. SPWLA-2010-58470.

Du, L., Walker, J. G., Pope, G. A., Sharma, M. M., & Wang, P. (2000). Use of Solvents to Improve the Productivity of Gas Condensate Wells. SPE 62935.

Kuenen, J. P. (1892). On Retrograde Condensation and the Critical Phenomena of Two Substances. Communications from the Physical Laboratory of the University of Leiden.

Kumar, V., Pope, G. A., & Sharma, M. M. (2006). Improving the Gas and Condensate Relative Permeability Using Chemical Treatments. SPE 100529.

Orangi, A., Nagarajan, N. R., Honarpour, M. M., & Rosenzweig, J. (2011). Unconventional Shale Oil and Gas-Condensate Reservoir Production, Impact of Rock, Fluid, and Hydraulic Fractures. SPE 140536.

Peng, D.Y., & Robinson, D. B. (1976). A New Two-Constant Equation of State. Industrial & Engineering Chemistry Fundamentals, 15(1), 59–64.

Rahimi, P., Cooper, S., & Alem, T. (2009). Diluent Evaluation for Bitumen Pipelining. The 5. NCUT Upgrading and Refining Conference 2009.

Sayed, M. A., & Al-Muntasheri, G. A. (2016). Mitigation of the Effects of Condensate Banking: A Critical Review. SPE Production and Operations, 31(2), 85–102.

Shanley, K. W., Cluff, R. M., & Robinson, J. W. (2004). Factors Controlling Prolific Gas Production from Low-Permeability Sandstone Reservoirs: Implications for Resource Assessment, Prospect Development, and Risk Analysis. AAPG Bulletin, 88(8), 1083–1121.

Whitson, C. H., & Brulé, M. R., Society of Petroleum Engineers. (2000). Phase Behavior. Henry L. Doherty Memorial Fund of AIME, Society of Petroleum Engineers.

Chapter 2 PVT Model

2.1 Model Selection

The pressure-volume-temperature (PVT) model captures the phase behaviour of the fluids (i.e. oil, gas, water and sometimes even solid) in reservoir simulation. The PVT model takes the measured PVT laboratory data as input and attempts to recover the phase behaviour of the reservoir fluid over a wide range of pressure and temperature. PVT models can be classified into two categories: black oil model and compositional model. The black oil model treats oil as a single component and represents its phase behaviour as a simple function of pressure solely, whereas the compositional model treats the fluids as several different components (either real chemical substances or virtual substances named pseudo-components) (Pedersen & Christensen, 2006). In a compositional model, the phase behaviour is usually thermodynamically computed from a cubic equation of state (EOS). The compositional models usually have better performance in simulating the phase behaviour of gas condensate for which drastic phase change can take place during the production process. But the black oil model bears much less computational cost.

In this thesis, a Peng-Robinson equation of state (PR-EOS) (Peng & Robinson, 1976) based compositional model with constant volume translation is established using CMG WINPROP to study the PVT behaviour and the pressure/temperature-dependent properties of a gas condensate fluid sample.

2.2 Data Collection

The model is built and calibrated based on the experimental data of a recombined North Sea gas condensate fluid sample reported by Whitson & Torp (Whitson & Torp, 1983). The fluid is a liquid-rich gas condensate with a dew point pressure of 6764.7 psi (46.64 MPa) at a reservoir

temperature of 280°F (138°C). The laboratory data include the compositional analysis of the fluid sample and constant volume depletion (CVD) test data. The CVD test is a standard PVT laboratory test to be conducted on a gas condensate sample. The CVD test simulates the isothermal pressure drawdown process of a gas condensate reservoir. **Table 2** summarizes the measured CVD test data on the North Sea gas condensate fluid.

Table 2. Measured CVD data of the North Sea gas condensate at 280°F (Whitson & Torp, 1983)

Pressure (psia)	Cumulative gas production (mole %)	Liquid dropout (volume %)	Compressibility factor of the gaseous phase
6764.7	0	0	n/a
5514.7	9.024	14.1	1.089
4314.7	21.744	19.7	0.972
3114.7	38.674	21.6	0.913
2114.7	55.686	21.3	0.914
1214.7	72.146	20.2	0.937
714.7	81.301	19.3	0.960

2.3 EOS-based Model Setup and Regression

The composition of the lighter components (i.e., C1-C6, N_2, and CO_2) is determined by Gas Chromatography (GC) in the compositional analysis. Due to the nature of GC, the compositional analysis cannot clearly distinguish a heavier component from others (Pedersen & Christensen, 2006). The heptane-plus (C7+) fraction of the fluid needs to be split and characterized by correlations. Exponential distribution and Kesler and Lee's correlations are used in the model to split and characterize the C7+ components (Lee and Kesler, 1975). The plus components are lumped into 5 pseudo-components (C7-C10, C11-C14, C15-C19, C20-C23, and C24+) for the simplicity of calculation. The compositions and properties of all the components are summarized

in **Table 3**. Regression of the following parameters has been carried out to match the CVD test data: the critical properties (i.e., P_c and T_c), the acentric factor (ω), and the volume translation of the pseudo-components and the binary interaction coefficients between CO_2/N_2/CH_4 and pseudo-components. It needs to be mentioned that the number of CVD data points is less than the number of regressed parameters. The results of the regression may not be unique. Certain boundaries were employed to ensure the validity of the model. Indeed, characterizing the heptane-plus with distribution already introduces new variables and uncertainty to the system. A unique and representation of the fluid sample may not be achievable with the limited data. The regressed properties are shown in red in **Table 3**. **Table 4** illustrates the binary interaction parameters that are obtained after regression. **Figure 2** compares the measured liquid dropouts against the simulated CVD test with the PR-EOS model. It can be observed from Figure 2 that the match of the CVD data has been significantly improved by the regression.

Table 3. Composition, critical temperature, critical pressure, acentric factor, and the dimensionless volume translation of the gas condensate sample. The parameters shown in red are the regressed values.

Component	Composition	T_c (K)	P_c (atm)	ω	Dimensionless volume translation
CO_2	2.37	304.2	73.76	0.225	-0.0817
N_2	0.31	126.2	33.94	0.040	-0.1927
C1	73.19	190.6	46.00	0.008	-0.1595
C2	7.80	305.4	48.84	0.098	-0.1134
C3	3.55	369.8	42.46	0.152	-0.0863
IC4	0.71	408.1	36.48	0.176	-0.0844
NC4	1.45	425.2	38.00	0.193	-0.0675
IC5	0.64	460.4	33.84	0.227	-0.0608
NC5	0.68	469.6	33.74	0.251	-0.0390
FC6	1.09	507.5	32.89	0.275	-0.0592
C07-C10	4.19	613.2	27.99	0.319	0.0431
C11-C14	1.68	594.0	17.82	0.458	-0.0547
C15-C19	1.10	662.1	16.45	0.634	-0.0052
C20-C23	0.48	808.4	13.47	0.989	0.1884
C24+	0.76	877.0	8.88	1.105	0.1534

Table 4. Binary interaction parameters used in the PVT model of the gas condensate model. The parameters that have been regressed are shown in red.

	CO2	N2	CH4	C2H6	C3H8	IC4	NC4	IC5	NC5	FC6	C07-C10	C11-C14	C15-C19	C20-C23	C24+
CO2	zero	0.000	0.105	0.130	0.125	0.120	0.115	0.115	0.115	0.115	0.150	0.150	0.150	0.150	0.150
N2	0.000	zero	0.025	0.010	0.090	0.095	0.095	0.100	0.110	0.110	0.120	0.120	0.120	0.120	0.120
CH4	0.105	0.025	zero	0.003	0.009	0.016	0.015	0.021	0.021	0.025	0.036	0.057	0.073	0.087	0.112
C2H6	0.130	0.010	0.003	zero	0.002	0.005	0.005	0.009	0.009	0.012	0.019	0.036	0.049	0.061	0.083
C3H8	0.125	0.090	0.009	0.002	zero	0.001	0.001	0.003	0.003	0.005	0.010	0.023	0.034	0.044	0.063
IC4	0.120	0.095	0.016	0.005	0.001	zero	0.000	0.000	0.000	0.001	0.004	0.014	0.023	0.031	0.048
NC4	0.115	0.095	0.015	0.005	0.001	0.000	zero	0.001	0.001	0.001	0.005	0.015	0.024	0.033	0.050
IC5	0.115	0.100	0.021	0.009	0.003	0.000	0.001	zero	0.000	0.000	0.002	0.010	0.017	0.025	0.040
NC5	0.115	0.110	0.021	0.009	0.003	0.000	0.001	0.000	zero	0.000	0.002	0.010	0.018	0.025	0.041
FC6	0.115	0.110	0.025	0.012	0.005	0.001	0.001	0.000	0.000	zero	0.001	0.007	0.014	0.020	0.035
C07-C10	0.150	0.120	0.036	0.019	0.010	0.004	0.005	0.002	0.002	0.001	zero	0.003	0.007	0.013	0.025
C11-C14	0.150	0.120	0.057	0.036	0.023	0.014	0.015	0.010	0.010	0.007	0.003	zero	0.001	0.004	0.011
C15-C19	0.150	0.120	0.073	0.049	0.034	0.023	0.024	0.017	0.018	0.014	0.007	0.001	zero	0.001	0.005
C20-C23	0.150	0.120	0.087	0.061	0.044	0.031	0.033	0.025	0.025	0.020	0.013	0.004	0.001	zero	0.002
C24+	0.150	0.120	0.112	0.083	0.063	0.048	0.050	0.040	0.041	0.035	0.025	0.011	0.005	0.002	zero

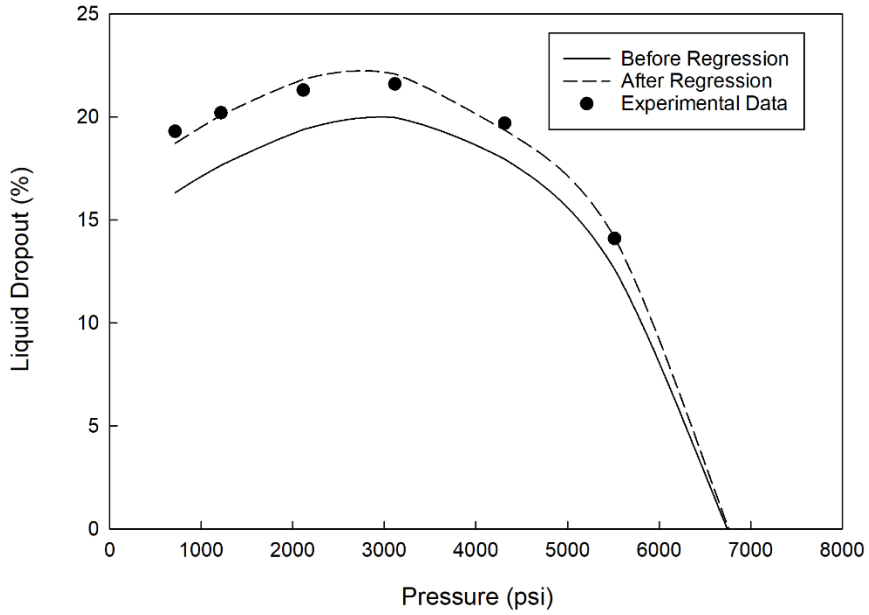

Figure 2. Liquid drop-out curves that are calculated using the PVT model before and after regression.

2.4 K-value Model Conversion

The STARS simulator developed by Computer Modeling Group Ltd. was used to investigate the effectiveness of using heat for condensate bank removal. The reason for choosing such a simulator is that STARS is capable of dealing with external heat sources while employing a K-value-based compositional PVT model (CMG Ltd., 2017). K-value, or the vapour-liquid equilibrium ratio, represents the ratio of the mole fraction of a component in the vapour phase to that in the liquid phase:

$$K_i = \frac{y_i}{x_i}$$

where y_i is the mole concentration of the component in the vapour phase, and x_i is the mole concentration of the component in the liquid phase.

A K-value table of the reservoir fluid can be generated by flash calculations using an EOS-based model at different pressures and temperatures, and the simulator uses the K-value table to approximate the PVT behaviour of the reservoir fluid. Compared with the EOS-based compositional simulation, the K-value-based simulation cannot perfectly capture the change of the in-situ fluid composition caused by the variations of compositions and flow rates in different phases. But it provides acceptable PVT estimations with significantly enhanced computational efficiency (Hong & Hsueh, 1987).

References

CMG Ltd. (2017). CMG STARS User Guide.

Hong, K. C., & Hsueh, L. (1987). Comparison of K-Value Calculation Methods in Compositional Steamflood Simulation. SPE Reservoir Engineering, 2(02), 249–257.

Lee, B.I., & Kesler, M.G. (1975). A Generalized Thermodynamic Correlation Based on Three-Parameter Corresponding States. AIChE Journal, 21(3), 510–527.

Pedersen, K. S., & Christensen, P. L. (2006). Phase Behavior of Petroleum Reservoir Fluids. CRC Press.

Peng, D.Y., & Robinson, D. B. (1976). A New Two-Constant Equation of State. Industrial & Engineering Chemistry Fundamentals, 15(1), 59–64.

Whitson, C. H., & Torp, S. B. (1983). Evaluating Constant-Volume Depletion Data. Journal of Petroleum Technology, 35(03), 610–620.

Chapter 3 Methodology

3.1 Reservoir Geometry

A two-dimensional cylindrical reservoir model as shown in **Figure 3** is built to investigate the proposed remedial method. A radial model is used to better capture the phase change and the fluid flow in the near-wellbore region. The reservoir model has an outer radius of 100 ft (30.48 m) with the production well in the centre. The inner radius of the reservoir is 0.3 ft which is the same as the wellbore radius. The width of the five most inner grid blocks is set to 1 ft (0.3048 m), and the width of the rest of the grid blocks increases logarithmically in the radial direction. The model consists of 10 identical layers in the vertical direction with a uniform thickness of 10 ft (3.048 m). All grid blocks cover 360° in the tangential direction (i.e., there is only one block in the tangential direction). A total of 200 grids are adopted in the simulation model. Grid independent analysis has been conducted to ensure the numerical accuracy of the model. No-flow boundary condition is used on the outer edge of the reservoir as well as the top and the bottom of the reservoir. The no-flow boundary condition ensures a continuous drawdown of the reservoir pressure, making it possible to simulate the complete depletion of the condensate reservoir.

The production well was placed in the centre of the reservoir with penetrations in all 10 layers. The downhole electrical heater and the electrode attached to the well also extend through all 10 layers in the reservoir. To study the effect of each remedial method at different stages of reservoir depletion, the bottomhole pressure of the production wells is set to 1000 psi (6.89 MPa), and the reservoirs are allowed to deplete freely for three years. For the gas injection cases, the well is put on production for 5 months followed by 1 month of injection at 10000 psi (68.95 MPa) bottomhole pressure. The maximum surface gas rate during injection is capped at 200,000 ft^3/day.

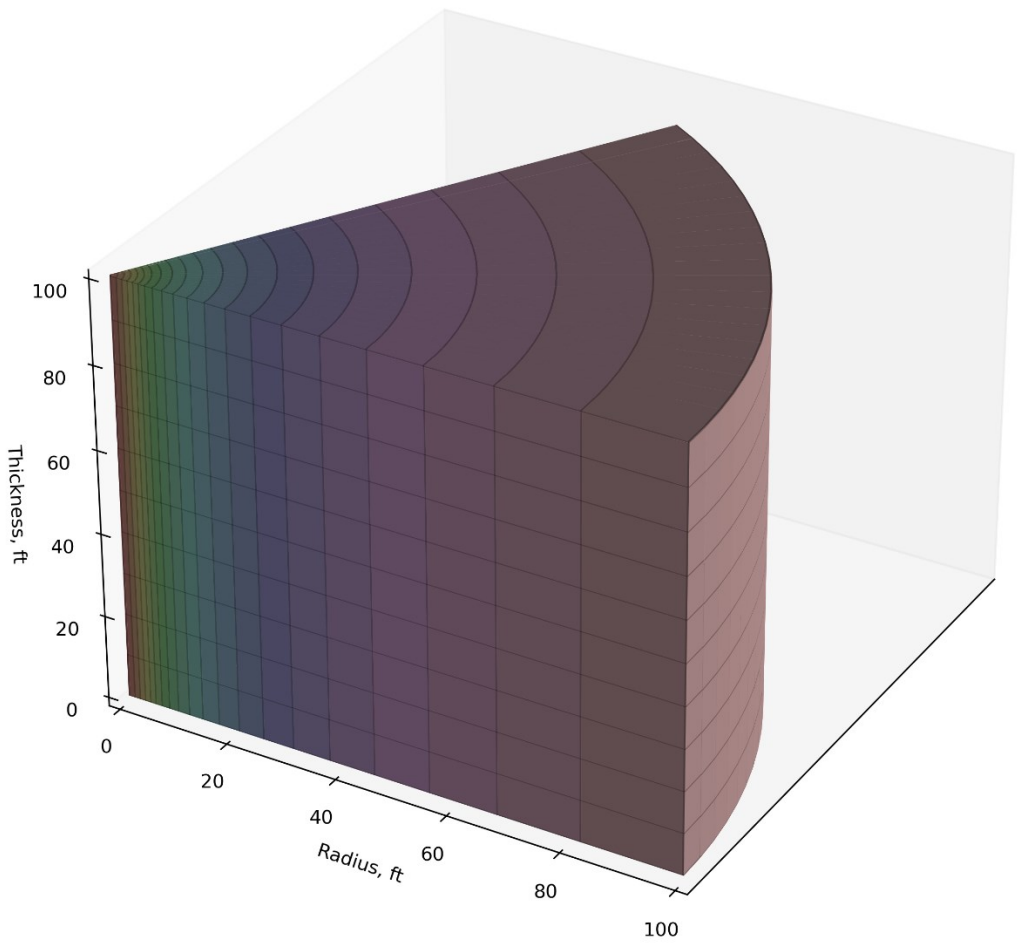

Figure 3. 3D schematic of the cylindrical reservoir model built for simulating the condensate removal methods. The plot only shows a slice of the reservoir. The real grid blocks cover 360° in the tangential direction.

3.2 Simulation Parameters

Flow in shale and tight sandstones is quite complex due to the presence of natural and hydraulic fractures. Dual-porosity or dual-permeability models are usually used to capture the effect of fracture flow. However, the geological conditions of real reservoirs differ from one case to another. It requires more elaborate studies on the natural fractures and matrix of an individual reservoir to develop the dual-porosity/dual-permeability model. The purpose of this research is to develop a

conceptual model to study the heating-based remedial methods and their influencing factors. Thus, the study uses a conventional single permeability model. The reservoir model uses homogeneous porosity. The permeability is anisotropic with the vertical permeability being 1/10 of the horizontal permeability. The detailed parameters of the reservoir model are summarized in **Table 5**. Parameters employed in the model are based on the typical values of shale/tight sandstone formations.

Table 5. Properties of the reservoir simulation model and simulation parameters.

Parameter	Value
Porosity	0.08
Initial pressure	8000 psi (55.2 MPa)
Initial temperature	280 °F (137.8 °C)
Water saturation	0.25
Formation compressibility	$5x10^{-6}$ 1/psi ($7.25x10^{-5}$ 1/kPa)
Reservoir rock volumetric heat capacity	43.8 Btu/ft3/°F ($2.94x10^{6}$ J/m3/K)
Reservoir rock thermal conductivity	14.8 Btu/ft/day/°F (1.07 W/m/K)
Over-burden/under-burden volumetric heat capacity	43.8 Btu/ft3/°F ($2.94x10^{6}$ J/m3/K)
Over-burden/under-burden thermal conductivity	14.8 Btu/ft/day/°F (1.07 W/m/K)
Gas/oil viscosity	Generated by using correlations[a]
Well radius	0.3 ft (91.44 mm)

a: (Fong & Nghiem,1980; Reid et al., 1977)

3.3 Relative Permeability

Relative permeability plays the most important role in evaluating the production loss from condensate banking (Hinchman & Barree, 1985). However, limited experimental measurements of relative permeability of low-permeability shale and tight sandstones are available due to numerous technical difficulties, such as the extremely long elapsing time of the experiments,

difficulties associated with rock sampling due to the fragile nature of the rock, and difficulties in restoring the in-situ reservoir conditions (Li et al., 2020; Moghaddam & Jamiolahmady, 2019). Another issue of the lab measurements that significantly impairs its practicability is that the relative permeability of the gas condensate reservoir does not depend solely on saturation (Guo et al., 2015). The fundamental mechanism of removing the gas condensate banking is that the displacing force works against the capillary force that holds condensate in the pores. The relative permeability is a strong function of the ratio of the two forces acting on the trapped phase, which is usually expressed as a dimensionless group called capillary number (Fulcher Jr. et al., 1985):

$$C_a = \frac{\mu V}{\sigma}$$

where μ is the dynamic viscosity, V is the fluid velocity, and σ is the interfacial tension. In this study, we use a relative permeability model on the basis of trapping number, which is a generalized form of capillary number as developed by Pope et al. (2000) to characterize the capillary effect. **Figure 4** shows the relative permeability curves used in the reservoir simulations. Parameters used to construct such curves are: $T_c = 30000$, $T_g = 50000$, $\tau_c = 1$, $\tau_g = 1$, $S_{cr}^{high} = 0$, $S_{cr}^{low} = 0.3$, $S_{gr}^{high} = 0$, $S_{gr}^{low} = 0.2$, $k_{rc}^{0\,high} = k_{rc}^{0\,low} = 1$, $k_{rg}^{0\,high} = 1$, and $k_{rg}^{0\,low} = 0.6$. Corey-like relative permeability models (Ward & Morrow, 1987) are used for generating the baseline relative permeabilities. The details of the permeability models are summarized in the Appendix.

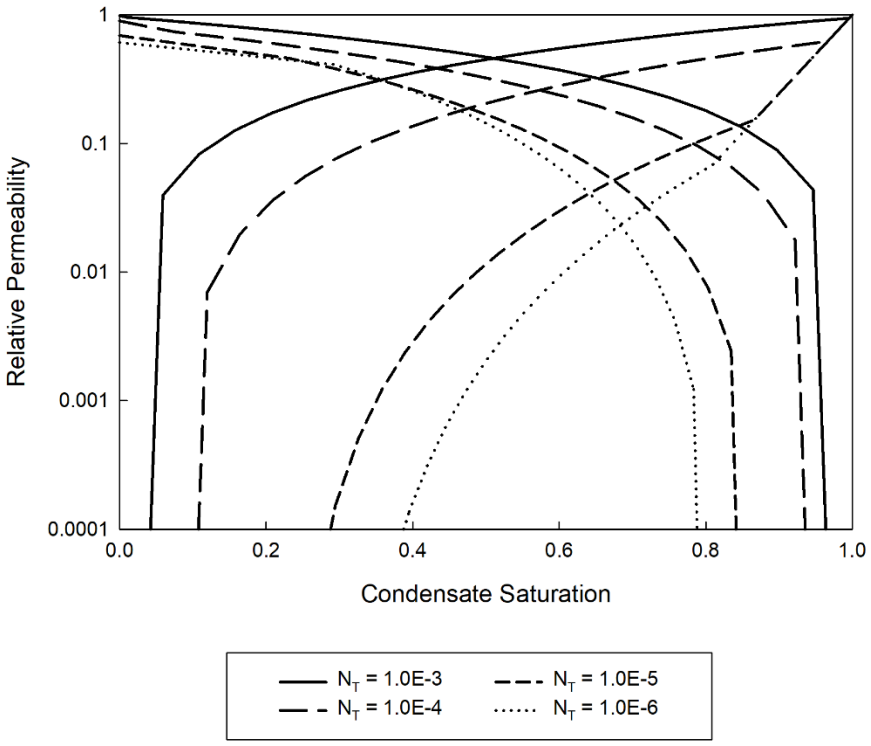

Figure 4. Relative permeability curves calculated from the trapping-number-based relative permeability model. N_T is the trapping number.

3.4 Simulation Schemes

In this research, we set up reservoir simulations to study the feasibility of the heating remedial method and compare it with the gas injection method. A total of 23 simulations of different scenarios were run. The details are summarized in **Table 6**. The simulations were run in 3 different permeability values: 0.01, 0.1, and 1 mD of horizontal permeability. Three simulations were run as the controlled group where the well was allowed to be depleted freely at 1000 psi bottomhole pressure and no other operations were applied. Seven simulations of DHEH at different permeabilities and heating power were run to study their effects on the performance. Seven more simulations of ERH in the same scenarios were run in order to compare the two heating methods. Six simulations of gas injections were run as a benchmark to study how the heating methods would perform compared with the conventional gas injection methods.

Table 6. Key parameters and descriptions of the simulation scenarios considered in the reservoir simulations. k_i refers to the absolute permeability along the horizontal direction, while P is the heating power.

Simulation index	Group	Key parameters	Descriptions
1	Controlled group	k_i = 0.01 mD	The well is allowed to be depleted freely with a bottomhole pressure of 1000 psi for three years. No heating is applied.
2		k_i = 0.1 mD	
3		k_i = 1 mD	
4	Downhole electrical heater heating	k_i = 0.01 mD; P = 5 kW	Heat is generated at the wellbore. The heating is treated directly as a source term in the well cell. The heat is evenly distributed over all penetrated cells.
5		k_i = 0.01 mD; P = 10 kW	
6		k_i = 0.01 mD; P = 20 kW	
7		k_i = 0.1 mD; P = 5 kW	
8		k_i = 0.1 mD; P = 10 kW	
9		k_i = 0.1 mD; P = 20 kW	
10		k_i = 1 mD; P = 10 kW	
11	Electrical resistance heating	k_i = 0.01 mD; P = 5 kW	Electrodes are installed across the production layers around the wellbore. Heat is generated by the current passing through the reservoir. In the simulation, the maximum allowed potential of the electrode is set to 220 V and the potential of the outer boundary of the reservoir is set to 0. The electrode potential is adjusted to match the desired heating power. The potential in grid blocks is estimated by solving charge conservation and Ohm's Law. The heat generated from ohmic loss is
12		k_i = 0.01 mD; P = 10 kW	
13		k_i = 0.01 mD; P = 20 kW	
14		k_i = 0.1 mD; P = 5 kW	
15		k_i = 0.1 mD; P = 10 kW	
16		k_i = 0.1 mD; P = 20 kW	

17		k_i = 1 mD; P = 10 kW	treated as source terms in each grid block.
18	Cyclic CH_4 injection	k_i = 0.01 mD	The well is allowed to deplete with a bottom hole pressure of 1000 psi for 5 months. And gas is injected at 10000 psi bottomhole pressure for 1 month. Afterwards, the process is repeated. The constraints applied on the injector ensure a similar energy consumption of the 0.01 mD cases to the 5 kW heating cases. The energy consumed in each 6-month period is approximately 80 GJ by assuming isothermal compression and ideal gas behaviour of the injecting gas.
19		k_i = 0.1 mD	
20	Cyclic N_2 injection	k_i = 0.01 mD	
21		k_i = 0.1 mD	
22	Cyclic CO_2 injection	k_i = 0.01 mD	
23		k_i = 0.1 mD	

3.5 NPV Analysis

NPV analysis provides an effective means of evaluating the economic feasibility and profitability of a project (Khan & Jain, 1999). NPV combines a series of expected cash flows and the time value of money, giving the anticipated return of an investment in terms of the present cash value. The NPV can be calculated as:

$$NPV = \sum_{t=0}^{n} \frac{R_t}{(1+i)^t}$$

where t is the number of periods, R_t is the net cash flow during the period t, and i represents the discount rate.

3.6 EROI

EROI or sometimes Energy Returned on Energy Invested (ERoEI) is a key metric of the efficiency and environmental impact of an energy source (Hall et al., 2014). EROI can be expressed as the

ratio of the amount of deliverable energy from an energy resource to the amount of energy used to exploit that resource (Hall et al., 2014):

$$ERoEI = \frac{Energy\ Delivered}{Energy\ Consumed\ to\ Deliver\ That\ Energy}$$

Any operation that has an EROI greater than 1 could result in a gain of energy, but the value needs to be greater than 3 for an operation to be considered economical and environmentally acceptable (Atlason & Unnthorsson, 2014). As a reference, the EROI of conventional hydrocarbon resources falls in the range of around 18 to 43 (Cleveland & O'Connor, 2011), whereas that of unconventional hydrocarbon resources is usually much lower. We are expecting somewhere around 5 for shale oil and 2 to 4 for bitumen (Murphy & Hall, 2010).

References

Atlason, R., & Unnthorsson, R. (2014). Ideal EROI (Energy Return on Investment) Deepens The Understanding of Energy Systems. Energy, 67, 241–245.

Cleveland, C. J., & O'Connor, P. A. (2011). Energy Return on Investment (EROI) of Oil Shale. Sustainability, 3(11), 2307–2322.

Fong, D.K.S., & Nghiem, L.X. (1980) A Viscosity Model for Reservoir Fluids. Computer Modelling Group Research Report R7.02.

Fulcher Jr., R. A., Ertekin, T., & Stahl, C. D. (1985). Effect of Capillary Number and Its Constituents on Two-Phase Relative Permeability Curves. Journal of Petroleum Technology, 37(02), 249–260.

Guo, H., Wang, F., Li, Y., Yu, Z., Gao, X., Gu, Y., Chen, J., Feng, S., & Zhang, X. (2015). Progress on Flow Mechanism in Low Permeability Formation. Procedia Engineering, 126, 466–470.

Hall, C. A. S., Lambert, J. G., & Balogh, S. B. (2014). EROI of Different Fuels and The Implications for Society. Energy Policy, 64, 141–152.

Hinchman, S. B., & Barree, R. D. (1985). Productivity Loss in Gas Condensate Reservoirs. SPE 14203.

Khan, M. Y., & Jain, P. K. (1999). Theory and Problems in Financial Management. Tata McGraw-Hill Education.

Li, R. Chen, Z., Wu, K., Liu, X., Dou, L. Yang, S., & Xu, J. (2020). A Fractal Model for Gas-Water Relative Permeability Curve in Shale Rocks. Journal of Natural Gas Science and Engineering. 81, 103417.

Moghaddam, R. N., & Jamiolahmady, M. (2019). Steady-State Relative Permeability Measurements of Tight and Shale Rocks Considering Capillary End Effect. Transport in Porous Media, 128, 75–96.

Murphy, D., Hall, C. (2010). Year in Review-EROI or Energy Return on (Energy) Invested. Annals of the New York Academy of Sciences, 1185, 102–118.

Pope, G., Wu, W., Narayanaswamy, G., Delshad, M., Sharma, M., & Wang, P. (2000). Modeling Relative Permeability Effects in Gas-Condensate Reservoirs with a New Trapping Model. SPE Reservoir Evaluation & Engineering, 3 (02), 171–178.

Reid, R.C., Prausnitz, J.M., & Sherwood, T.K. (1977). The Properties of Gases and Liquids, 3rd Edition, McGraw-Hill.

Ward, J. S., & Morrow, N. R. (1987). Capillary Pressures and Gas Relative Permeabilities of Low-Permeability Sandstone. SPE Formation Evaluation, 2(03), 345–356.

Chapter 4 Results & Discussion

4.1 Gas Injection Simulation Results

Gas injection, being one of the most common remedial methods for gas condensate banking, has been well applied and exhibited good performance in conventional reservoirs. This research first studies the changes to the phase behaviour of the reservoir fluid by adding three different injection gases. Afterwards, reservoir simulations of the gas injection operations are performed, serving as the benchmarks for further analysis of the proposed heating-based remedial methods.

4.1.1 Effects of Gas Injection on Phase Behaviour

Analyzing the phase behaviour changes to the reservoir fluid is one of the crucial works prior to the implementation of the gas injection operations. The analysis screens out the most suitable injection gas for a specific reservoir fluid.

With the PVT model established and regressed, we can easily change the composition of the mixture to model the change to the reservoir fluid's phase behaviour subjected to gas injection. CH_4, CO_2, and N_2 are examined in this section since they are some of the most commonly used injection gasses. **Figure 5** to **Figure 7** are the pressure-composition (P-x) phase envelopes of the gas condensate and CH_4/CO_2/N_2 mixtures. It is clearly seen from the figures that the two-phase region shrinks with the addition of CO_2 and enlarges with the addition of N_2. The injection of CH_4 slightly increases the dew point pressure at 280°F but also shrinks the 95% and 90% vapour region.

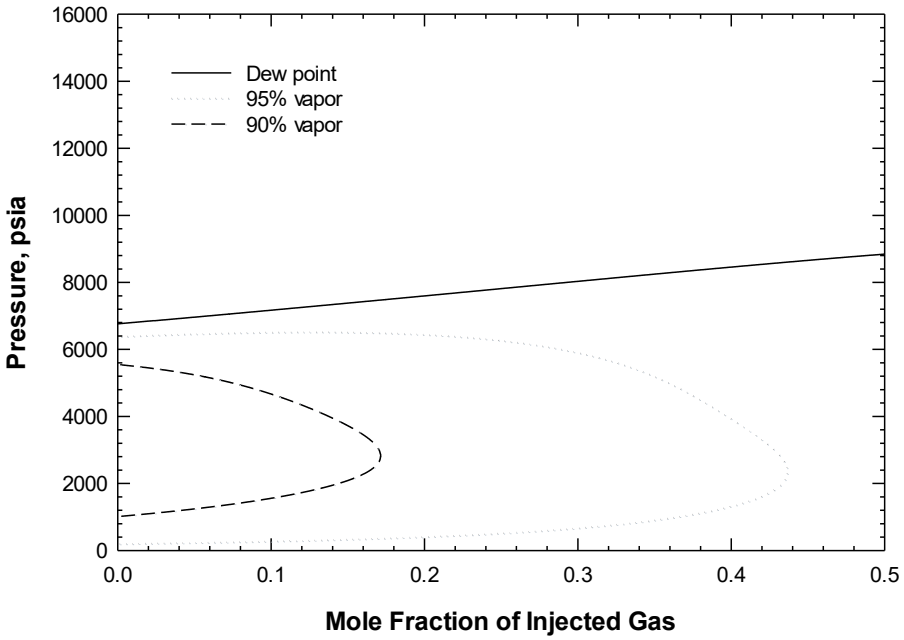

Figure 5. P-x phase envelope of the gas condensate and pure CH_4 system at 280°F.

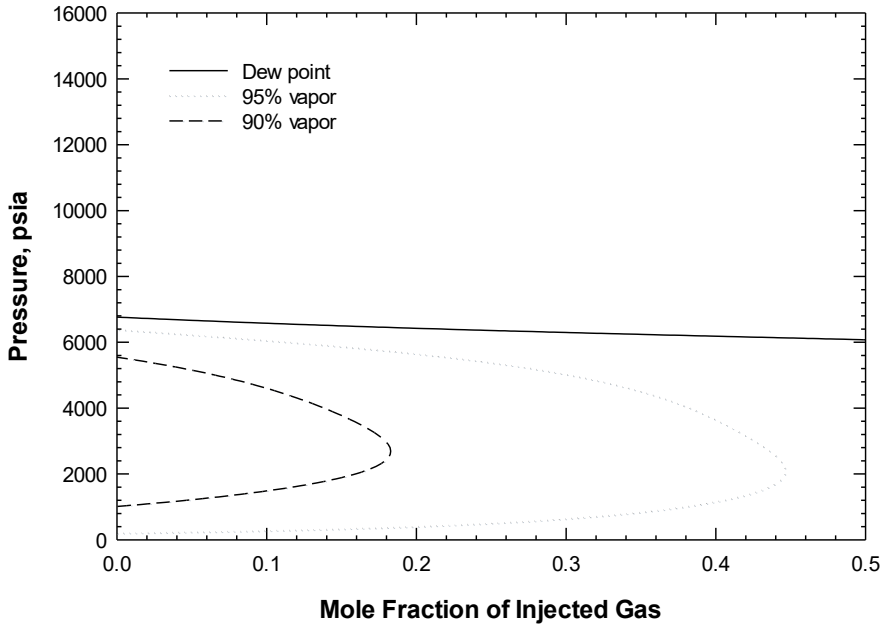

Figure 6. P-x phase envelope of the gas condensate and pure CO_2 system at 280°F.

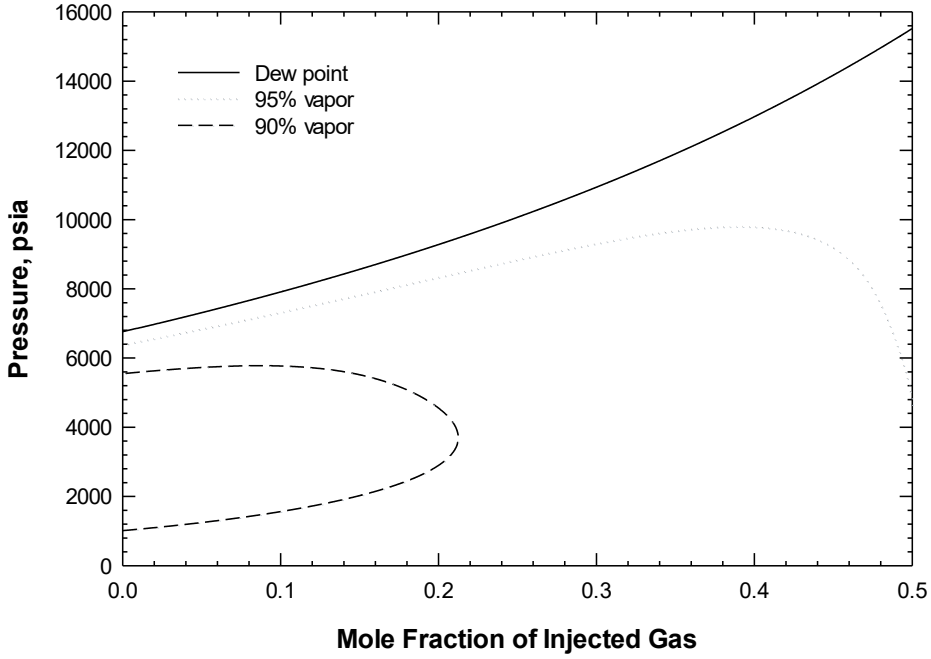

Figure 7. P-x phase envelope of the gas condensate and pure N_2 system at 280°F.

Even though N_2 is not a very good choice of injection gas in terms of shrinking the two-phase region, it can still be injected to restore and maintain the reservoir pressure. And it is much more accessible compared with CH_4 and CO_2. The injecting gases are usually combined to reduce the cost. **Figure 8** to **Figure 10** show the phase boundaries and saturation curves of the gas condensate and CH_4-CO_2 mixture systems. **Figure 11** to **Figure 13** show the phase boundaries and saturation curves of the gas condensate and CO_2-N_2 mixture systems. **Figure 14** to **Figure 16** show the phase boundaries and saturation curves of the gas condensate and CH_4-N_2 mixture systems. With the addition of CO_2 or CH_4 to N_2, the phase boundaries and saturation curves of the gas condensate-mixture system change significantly, which could potentially make the phase behaviour of the system favourable for gas injection.

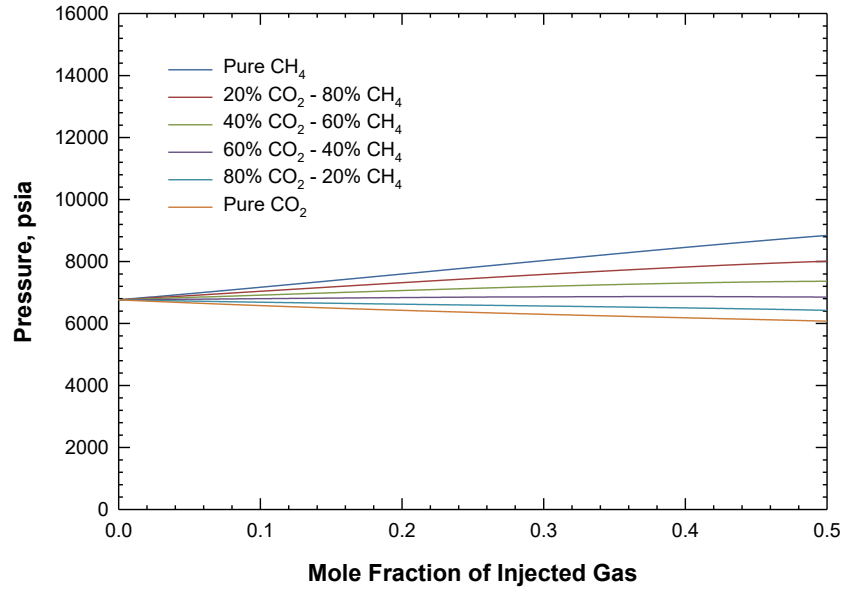

Figure 8. Dew point curves in the P-x phase envelopes of the gas condensate and CO_2-CH_4 mixture system at 280°F.

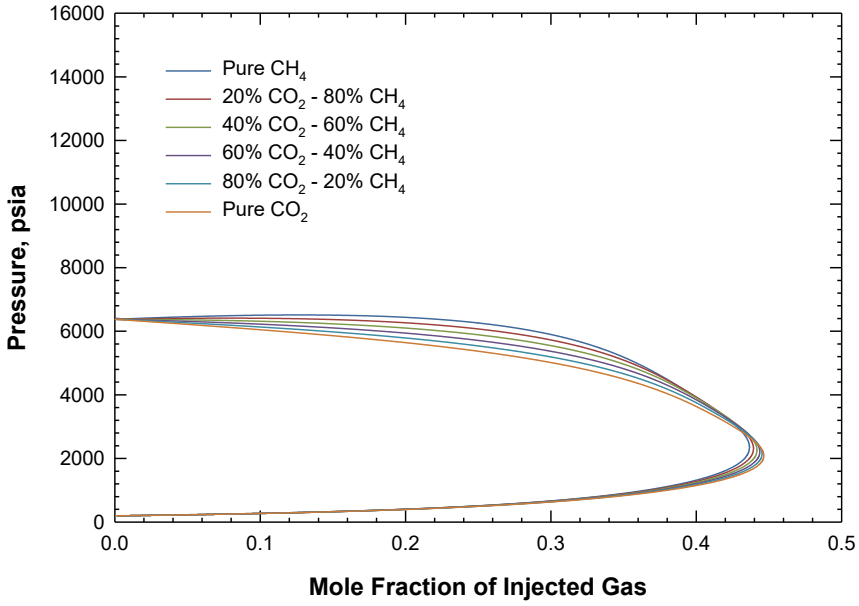

Figure 9. 95%-mole-fraction vapour saturation curves of the gas condensate and CO_2-CH_4 mixture system at 280°F.

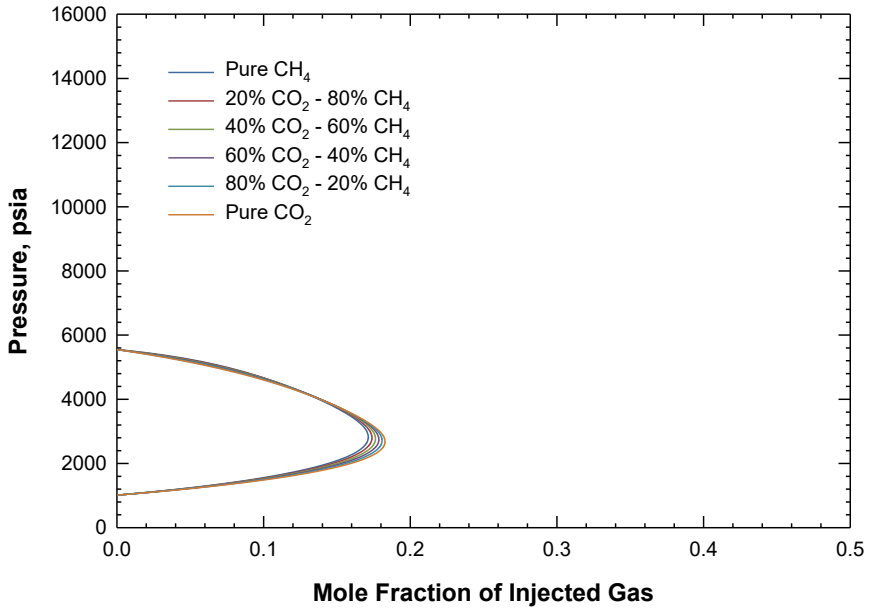

Figure 10. 90%-mole-fraction vapour saturation curves of the gas condensate and CO_2-CH_4 mixture system at 280°F.

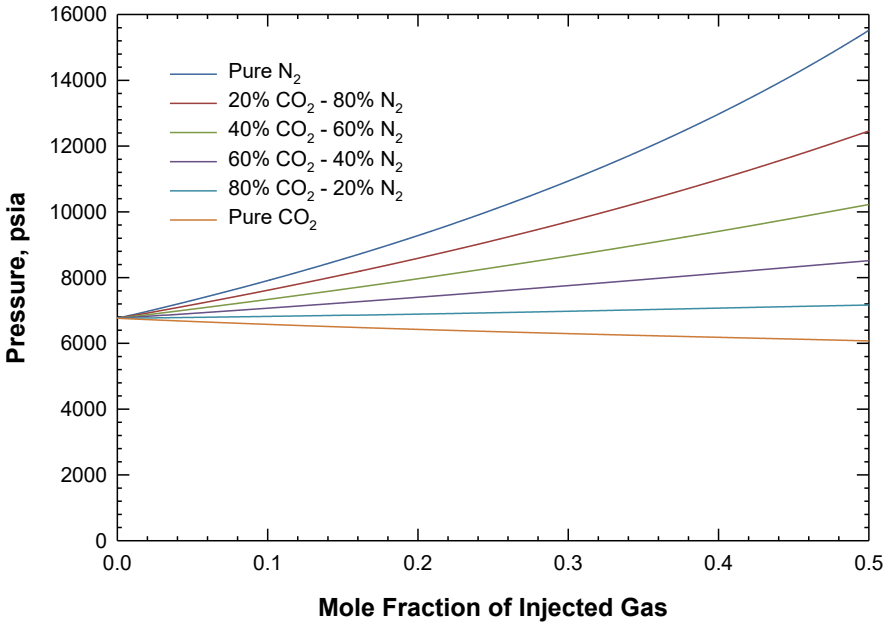

Figure 11. Dew point curves in the P-x phase envelopes of the gas condensate and CO_2-N_2 mixture system at 280°F.

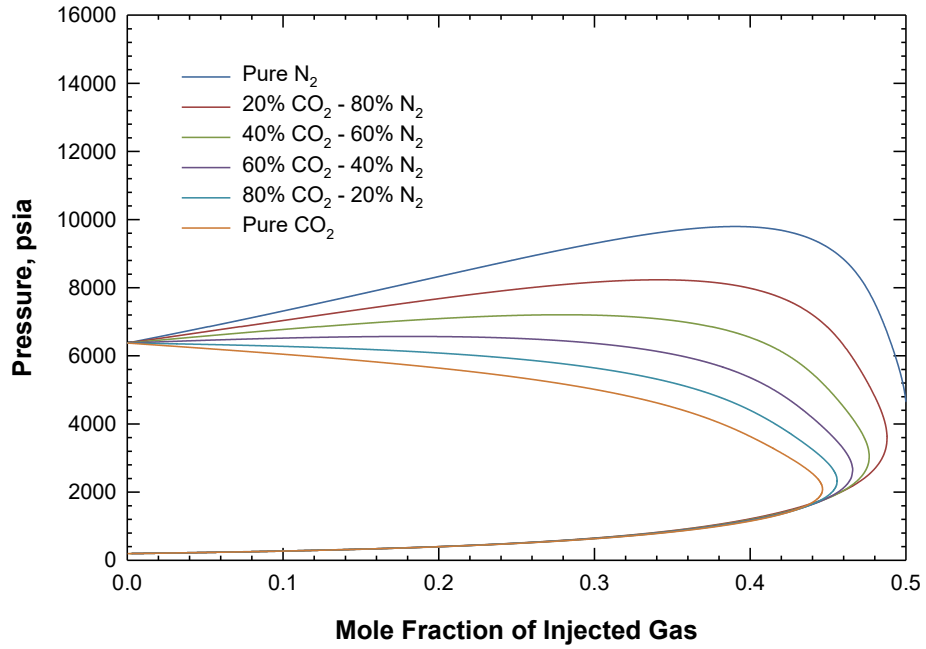

Figure 12. 95%-mole-fraction vapour saturation curves of the gas condensate and CO_2-N_2 mixture system at 280°F.

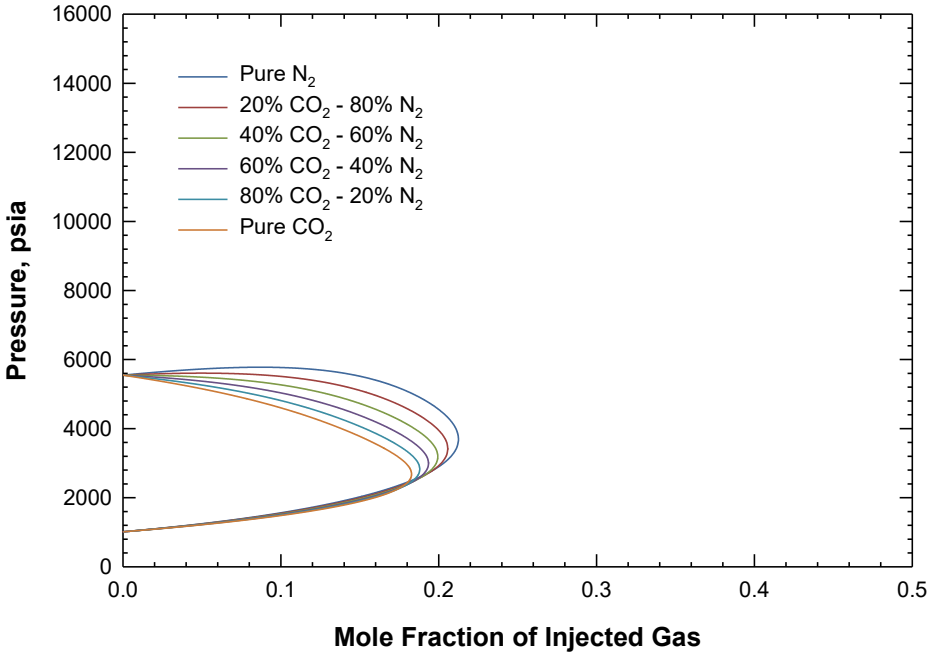

Figure 13. 90%-mole-fraction vapour saturation curves of the gas condensate and CO_2-N_2 mixture system at 280°F.

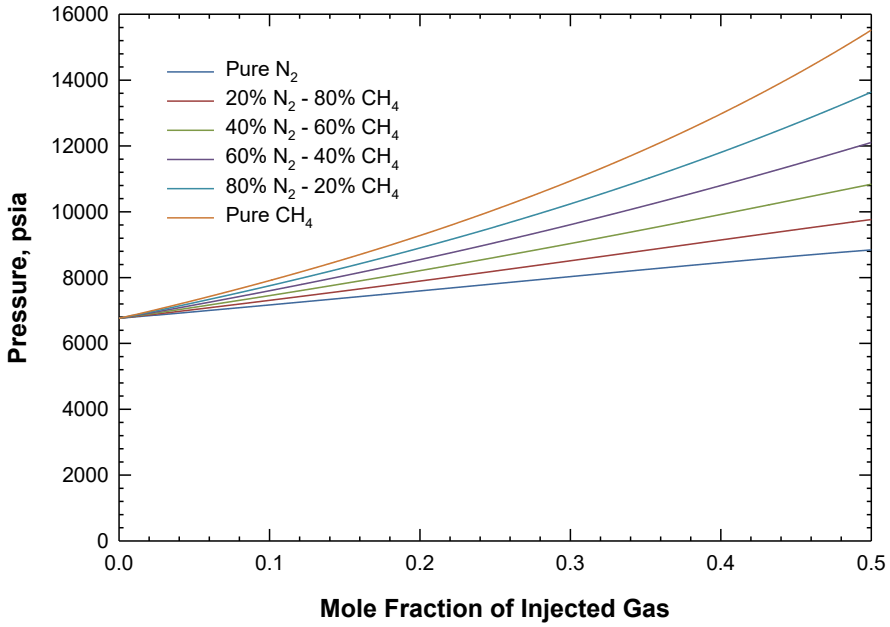

Figure 14. Dew point curves in the P-x phase envelopes of the gas condensate and N_2-CH_4 mixture system at 280°F.

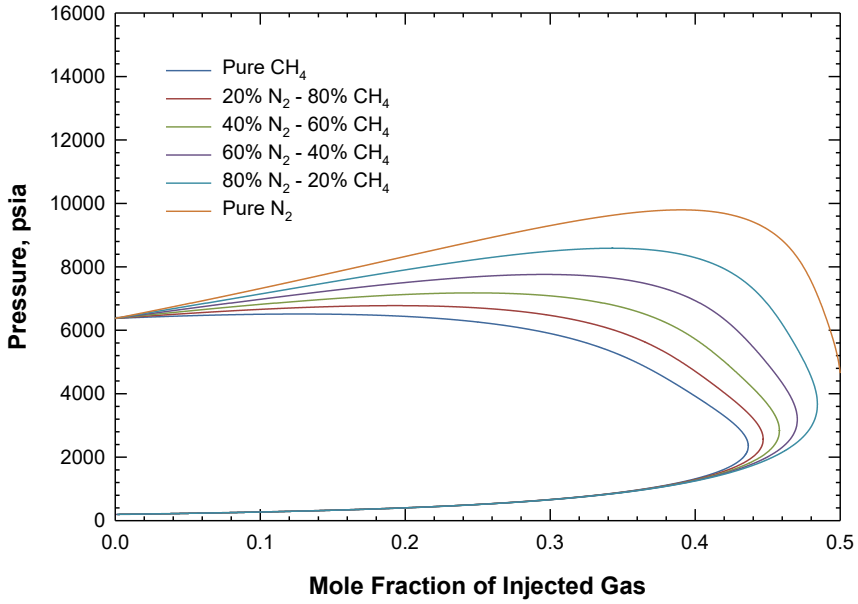

Figure 15. 95%-mole-fraction vapour saturation curves of the gas condensate and N_2-CH_4 mixture system at 280°F.

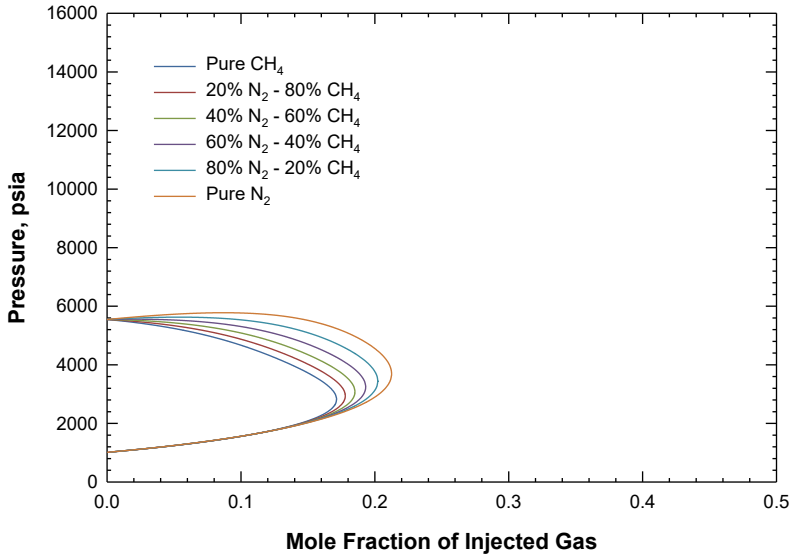

Figure 16. 90%-mole-fraction vapour saturation curves of the gas condensate and N_2-CH_4 mixture system at 280°F.

4.1.2 Reservoir Simulation on Gas Injection

Reservoir simulations examining the use of gas injection to remove the condensate bank are performed. The well is allowed to deplete with a bottomhole pressure of 1000 psi for 5 months, followed by 1 month of gas injection at a bottomhole pressure of 10000 psi. Afterwards, the process is repeated. The simulation results are presented in this section.

Figure 17 and **Figure 18** illustrate the gas production of the gas injection models in reservoirs of different permeabilities. The net cumulative gas production is calculated in such a way that the volume of the injected CH_4, CO_2, and N_2 or the volume of the produced CH_4, CO_2, and N_2, whichever is less, is deducted from the total cumulative gas production. By doing so, it avoids counting the production of the injected gas into the cumulative gas production. The three gas injection modes in **Figure 17** seem to outperform the case without gas injection and show similar performance in the first two injection-production cycles. After two cycles of production, the

reservoir is mostly depleted. N_2 injection seems to have a relatively better performance towards the end of the depletion.

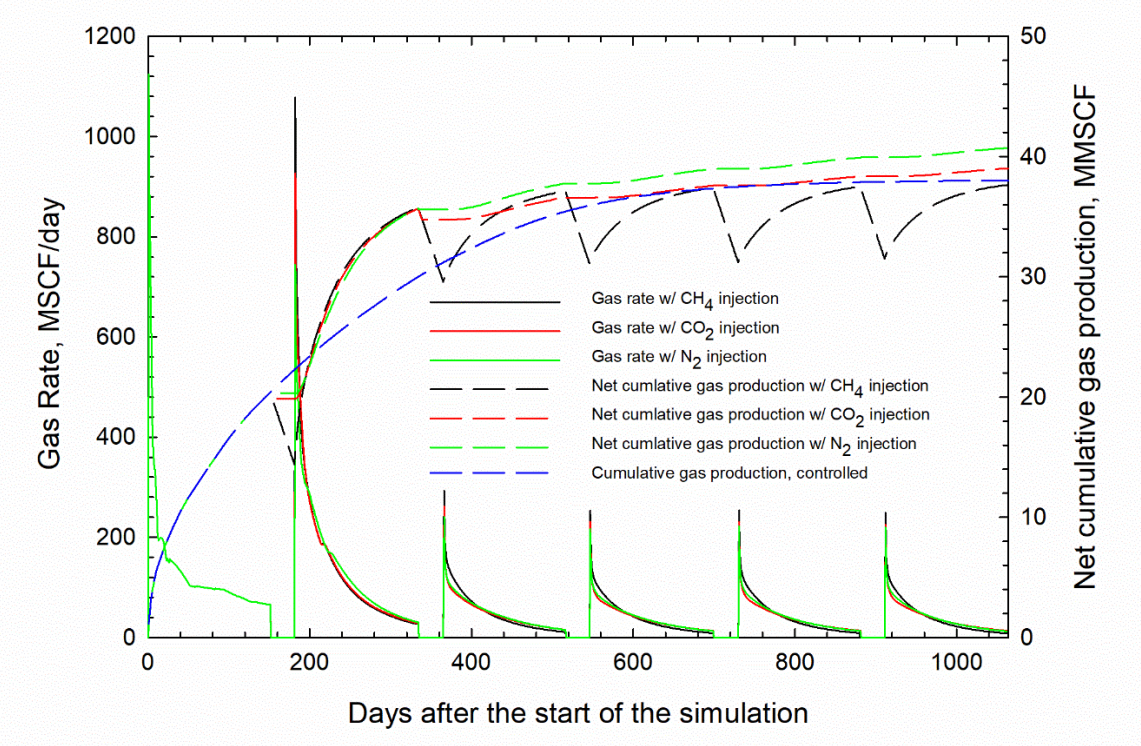

Figure 17. The gas production rate and net cumulative gas production of CH_4, CO_2, and N_2 injection in the 0.1 mD reservoir.

Figure 18 shows the gas production rate and net cumulative gas production of CH_4, CO_2, and N_2 injection in the 0.01 mD reservoir. As seen from Figure 18, the injection of CH_4 and CO_2 seems to have better performance to the gas production than the injection of N_2 throughout the simulation period. The stimulation effect by gas production becomes more obvious after a few production-injection cycles. The 0.1 mD reservoir is almost depleted after two production-injection cycles, while the 0.01 mD reservoir continues to be depleted after six cycles of treatment. Therefore, the

period, during which the gas injection stimulation remains effective, tends to be longer in reservoirs with lower permeability.

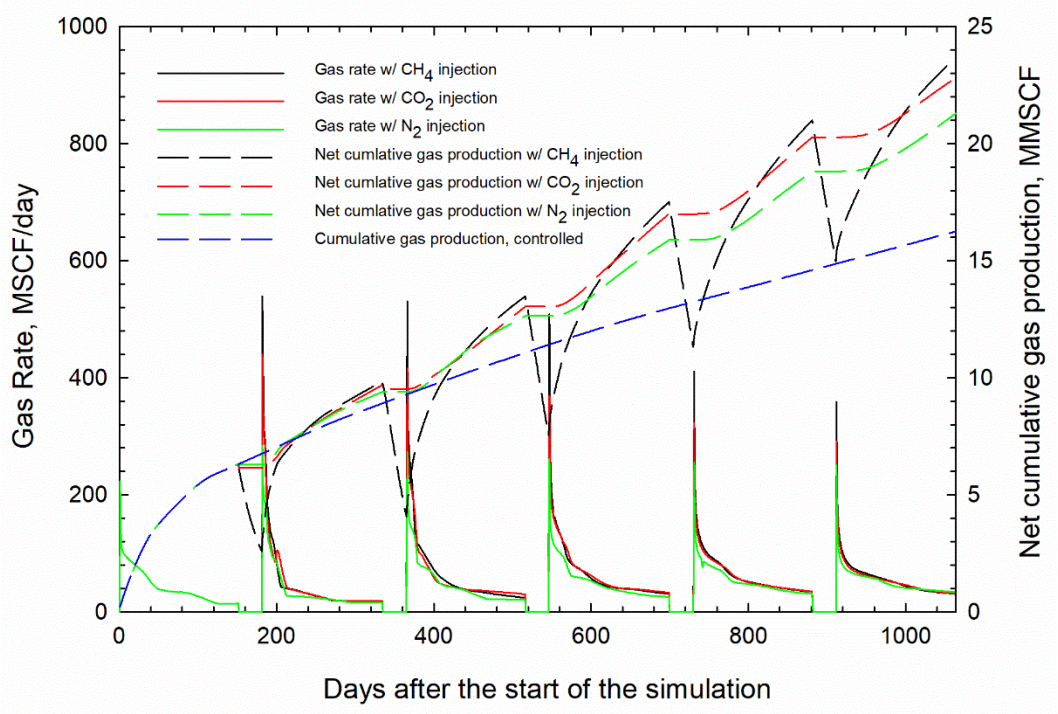

Figure 18. The gas production rate and net cumulative gas production of CH_4, CO_2, and N_2 injection in the 0.01 mD reservoir.

4.2 Reservoir Simulation on Electrical Heating

Although the simulation results shown above indicate that gas injection is an effective method for mitigating the condensate blockage issue, such a method would be very costly since extensive field operations are involved in gas injection operations. In this section, we present the simulation results on electrical heating and compare the effectiveness and performance of these two heating approaches based on the reservoir simulation results.

4.2.1 Gas and Condensate Production

By conducting the simulations, the fluid flow and heat transfer in the reservoir can be solved numerically. The gas and condensate produced at the surface condition can be calculated. **Figure 19** to **Figure 21** show the gas production rate and cumulative gas production of different heating schemes in the 0.01 mD reservoir. As seen from these figures, at the same heating power of 5 kW, the DHEH method shows a better performance than the ERH heating. Both methods perform similarly under 10 kW and 20 kW power settings. The overall gas production for all heated cases during the simulation period almost doubles that of the non-heated case. With a similar energy consumption, both heated approaches operated at 5 kW yields more gas production than the gas injection method in the 0.01 mD reservoir.

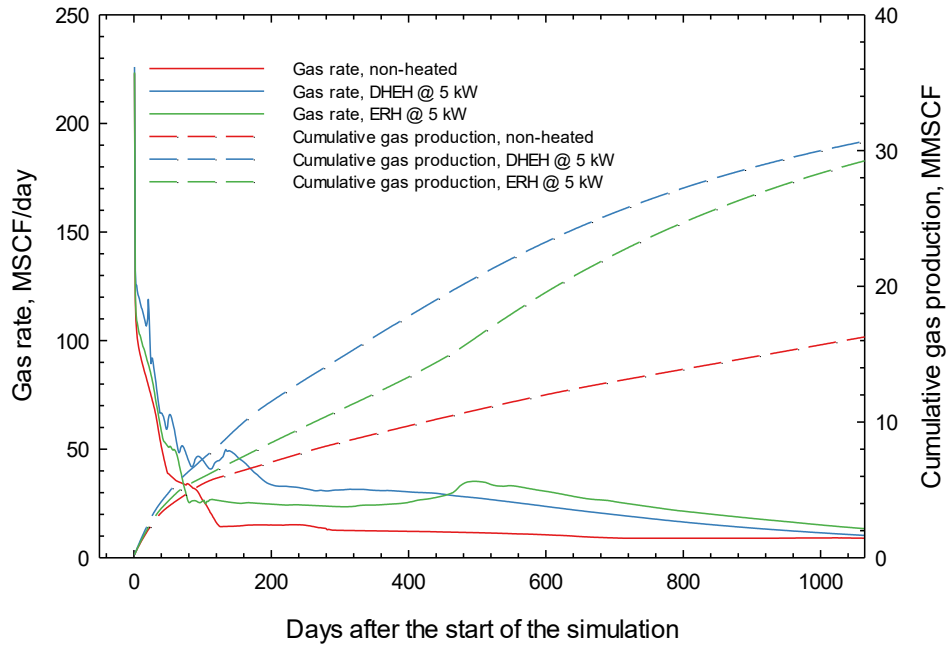

Figure 19. Gas production rate and cumulative gas production of the non-heated case and the DHEH and ERH cases operated at 5 kW in the 0.01 mD reservoir.

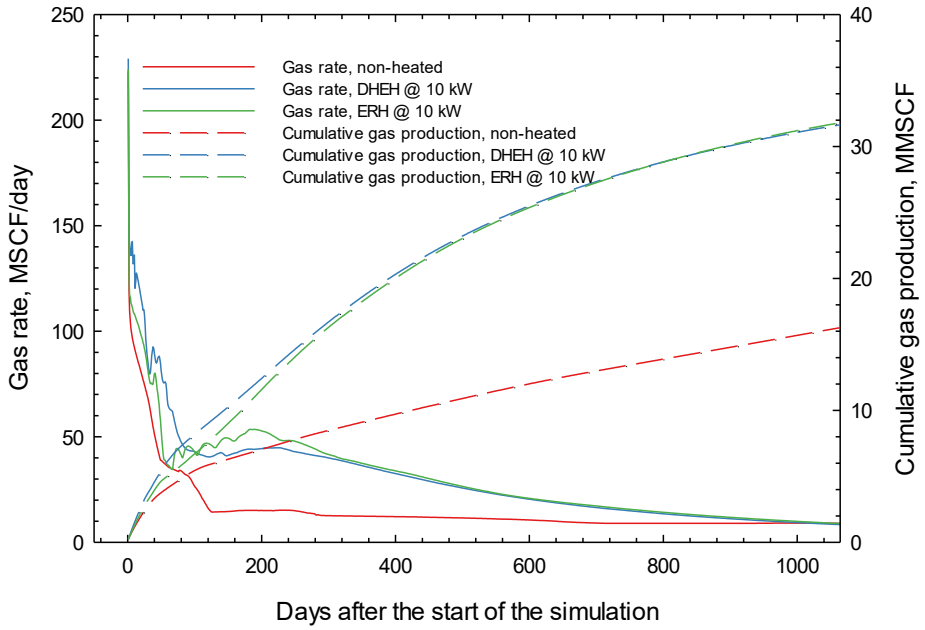

Figure 20. Gas production rate and cumulative gas production of the non-heated case and the DHEH and ERH cases operated at 10 kW in the 0.01 mD reservoir.

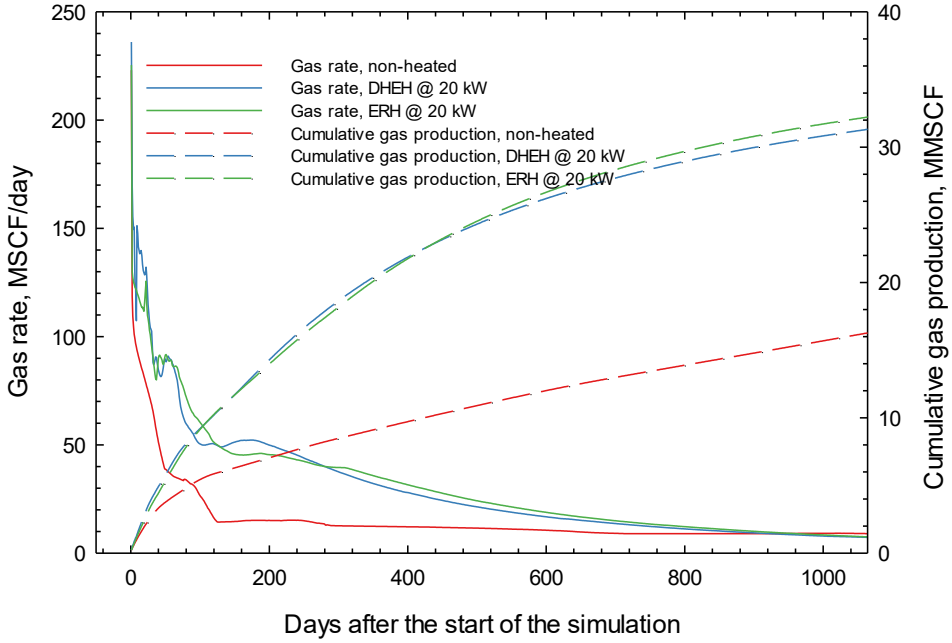

Figure 21. Gas production rate and cumulative gas production of the non-heated case and the DHEH and ERH cases operated at 20 kW in the 0.01 mD reservoir.

Figure 22 to **Figure 24** illustrate the gas production rate and the cumulative gas production of different heating schemes in the 0.1 mD horizontal permeability reservoir. Since the reservoir is relatively small, the reservoir completely depletes during the simulation period. However, significant production improvement still can be found in the early stages of production. It is also worth noting that, under a low heating power, the DHEH method shows a slightly better performance than the ERH method. But the ERH method outperforms the DHEH method under a higher heating power.

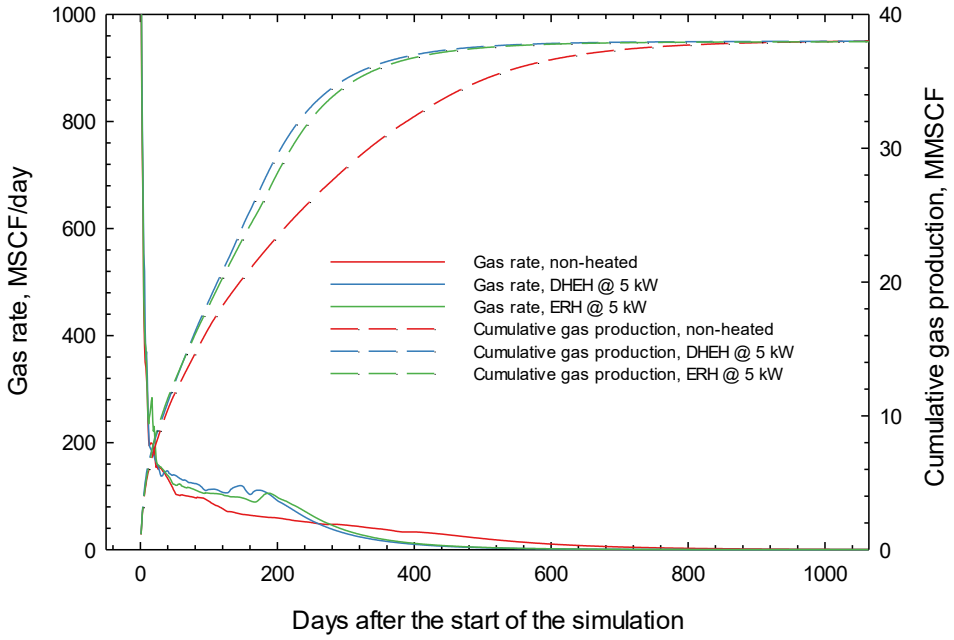

Figure 22. Gas production rate and cumulative gas production of the non-heated case and the DHEH and ERH cases operated at 5 kW in the 0.1 mD reservoir.

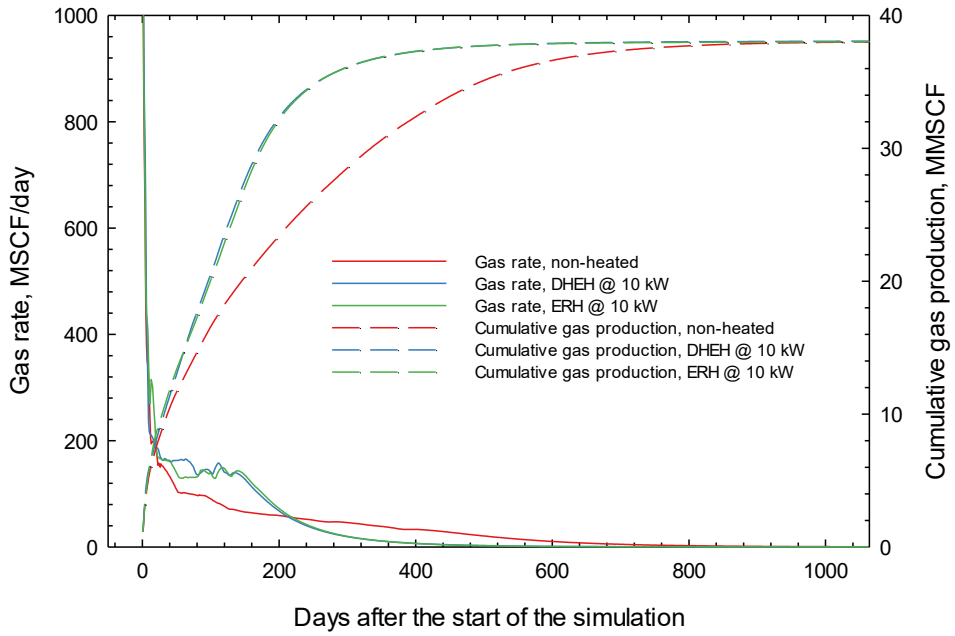

Figure 23. Gas production rate and cumulative gas production of the non-heated case and the DHEH and ERH cases operated at 10 kW in the 0.1 mD reservoir.

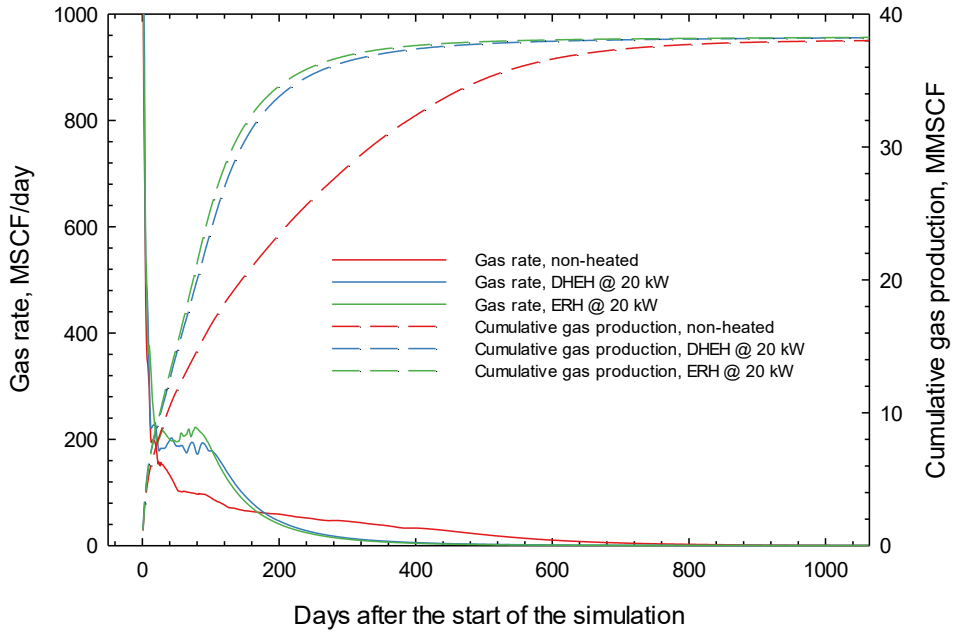

Figure 24. Gas production rate and cumulative gas production of the non-heated case and the DHEH and ERH cases operated at 20 kW in the 0.1 mD reservoir.

Figure 25 shows the gas production rate and the cumulative gas production of both heating methods in the 1 mD horizontal permeability reservoir. The reservoir depletes rapidly, and the heating operation seems to be not effective due to a very large gas influx.

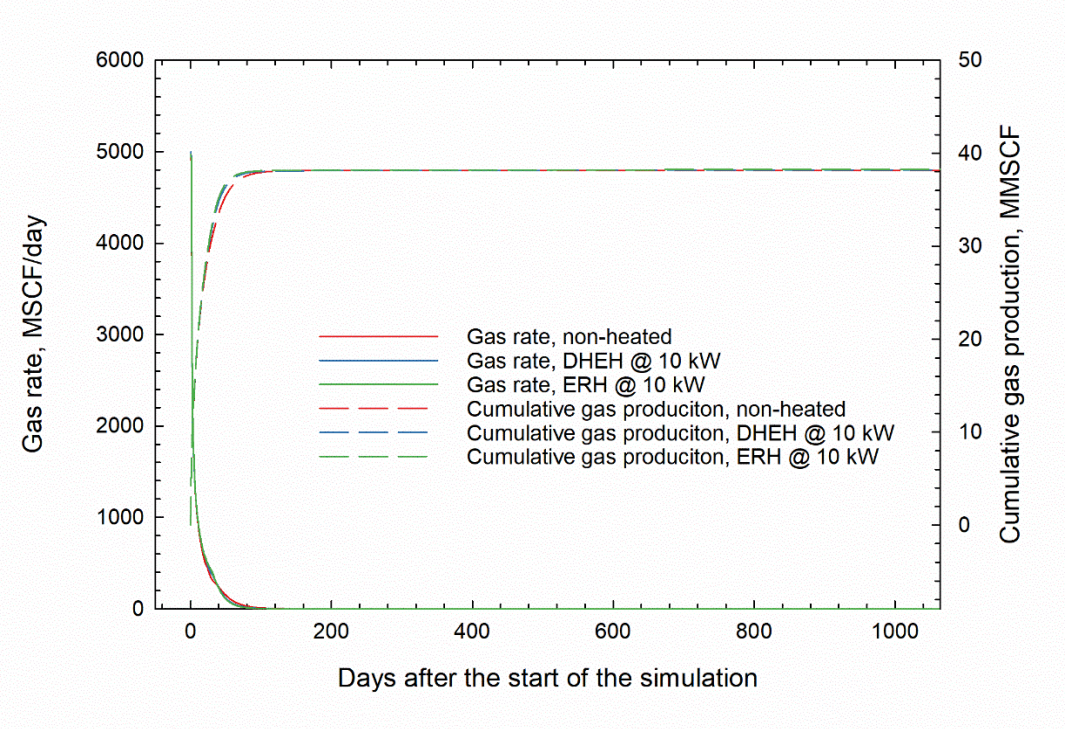

Figure 25. Gas production rate and cumulative gas production of the non-heated case and the DHEH and ERH cases operated at 10 kW in the 1 mD reservoir.

Figure 26 to **Figure 29** illustrate the gas oil ratio (GOR) and the cumulative oil (condensate) production of the non-heated case and the DHEH and the ERH cases with different operation power and different permeability. Heating operation increases the condensate production to different levels. However, the GOR of all heated cases in the 0.01 mD reservoir is also elevated from the non-heated case. The GOR of the heated cases in the 0.1 mD reservoir is higher than that of the non-heated case at the beginning, but declines as the reservoir depletes. It is worth noting

that the GOR of the ERH case operated at 5 kW in the 0.01 mD reservoir changes dramatically during the production. It starts with the lowest value. Then it rises quickly after about 500 days and ends up with being the highest among all the heated cases.

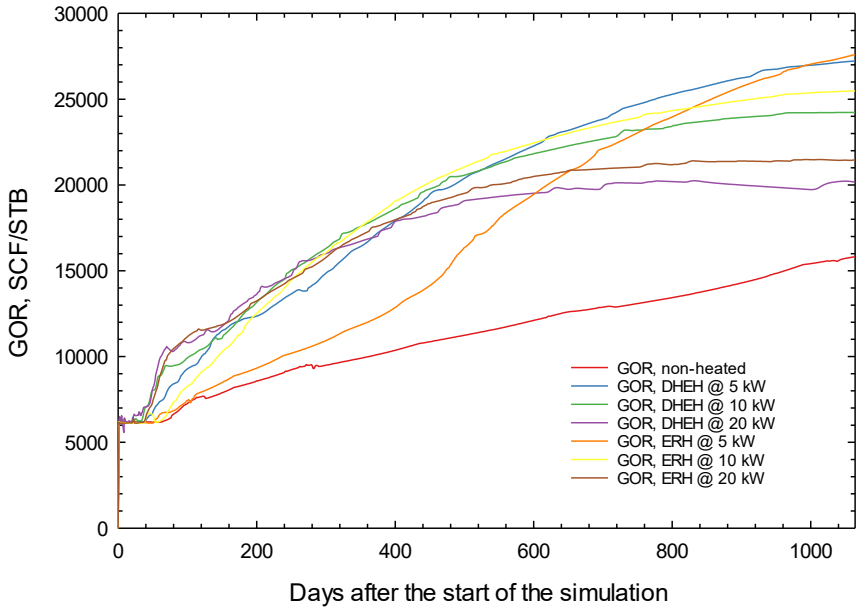

Figure 26. The gas oil ratio of the non-heated case and the DHEH and ERH cases operated at 5, 10 and 20 kW in the 0.01 mD reservoir.

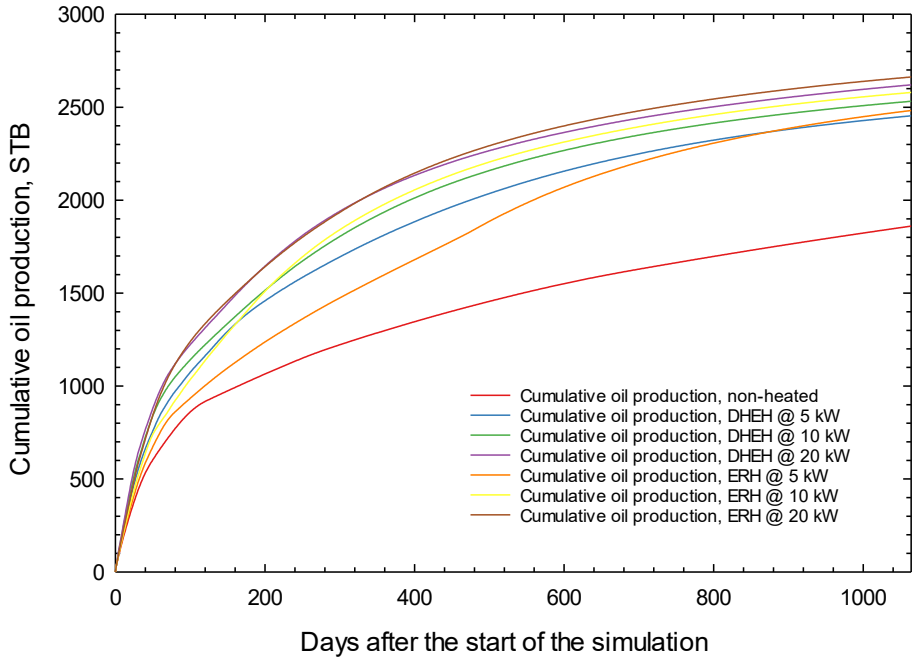

Figure 27. The cumulative oil production of the non-heated case and the DHEH and ERH cases operated at 5, 10 and 20 kW in the 0.01 mD reservoir.

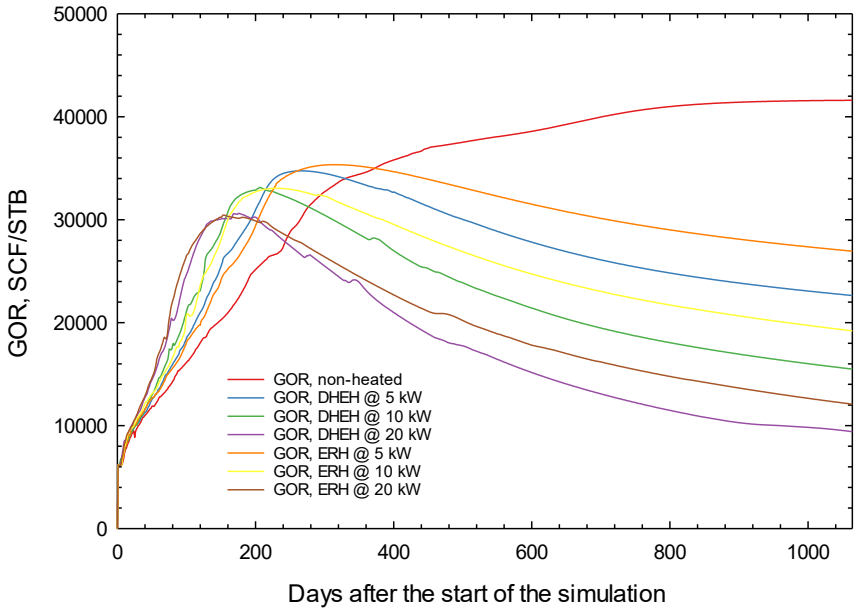

Figure 28. The gas oil ratio of the non-heated case and the DHEH and ERH cases operated at 5, 10 and 20 kW in the 0.1 mD reservoir.

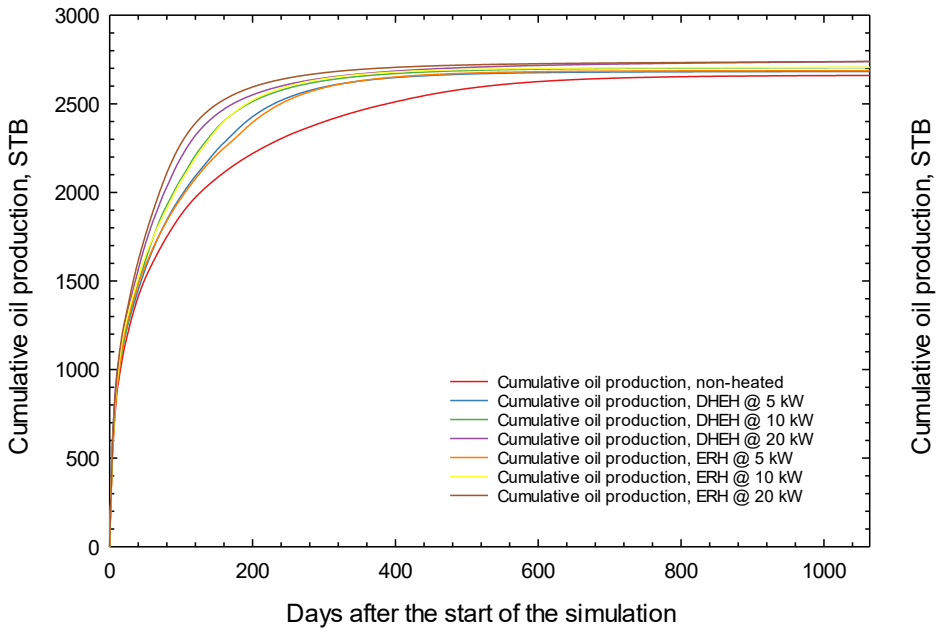

Figure 29. The cumulative oil production of the non-heated case and the DHEH and ERH cases operated at 5, 10 and 20 kW in the 0.1 mD reservoir.

In summary, the simulation results presented above demonstrate that, for the 0.01 mD reservoir model, both heating methods outperform the gas injection method by a significant margin; even with the lowest heating power of 5 kW, the effectiveness of heating treatments is found to be still higher than that of the best case in the gas injection schemes. As for the 0.1 mD reservoir, it would be inappropriate to directly compare the injection method against the heating method due to the short effective period.

4.2.2 Temperature and Saturation Profiles

Figure 30 illustrates the temperature profile of the DHEH, ERH, and non-heated cases at different times. The temperature of the non-heated model is slightly lower than the initial reservoir temperature near the wellbore due to pressure discharge phenomena. The temperature of the

DHEH model near the wellbore is higher than that of the ERH model. But the heat penetrates deeper into the reservoir in the ERH model. This result is expected as heat is generated in the wellbore in the DHEH method, while heat is generated in the reservoir in the ERH method. In this case, the heated area keeps expanding until at least 8 months after the start of the production when the depletion is almost completed for both heating methods.

Figure 31 shows the gas and water saturation profile of the DHEH, ERH, and non-heated cases at different times. Due to the heating, a small region of higher gas saturation is formed about 5 to 10 ft around the wellbore. This region expands as the high-temperature region expands, and the saturation difference between the heated and non-heated model become more significant towards the end of the depletion.

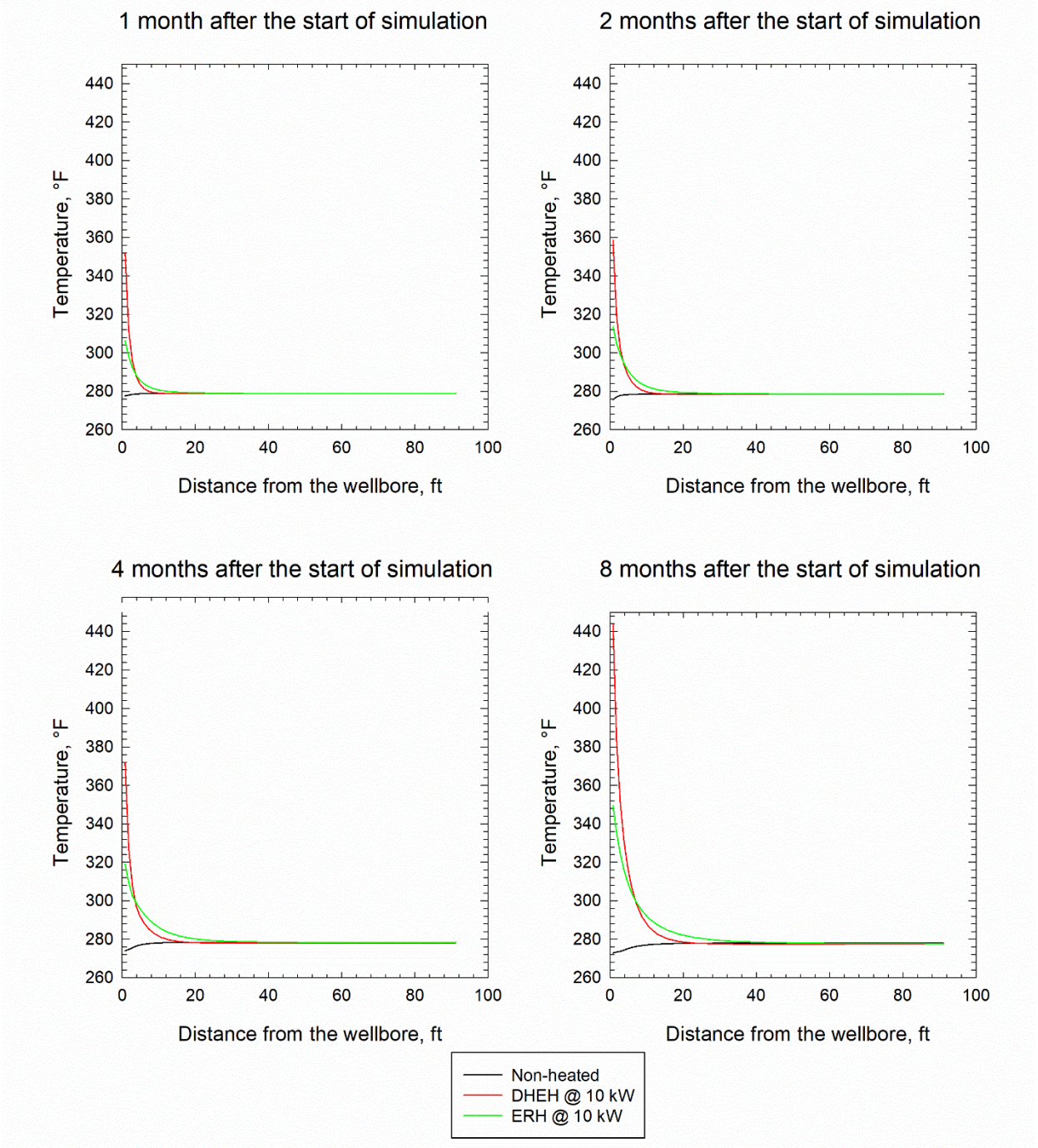

Figure 30. Temperature profile of the fifth layer in the 0.1 mD reservoir at 1, 2, 4, and 8 months after the start of the simulation.

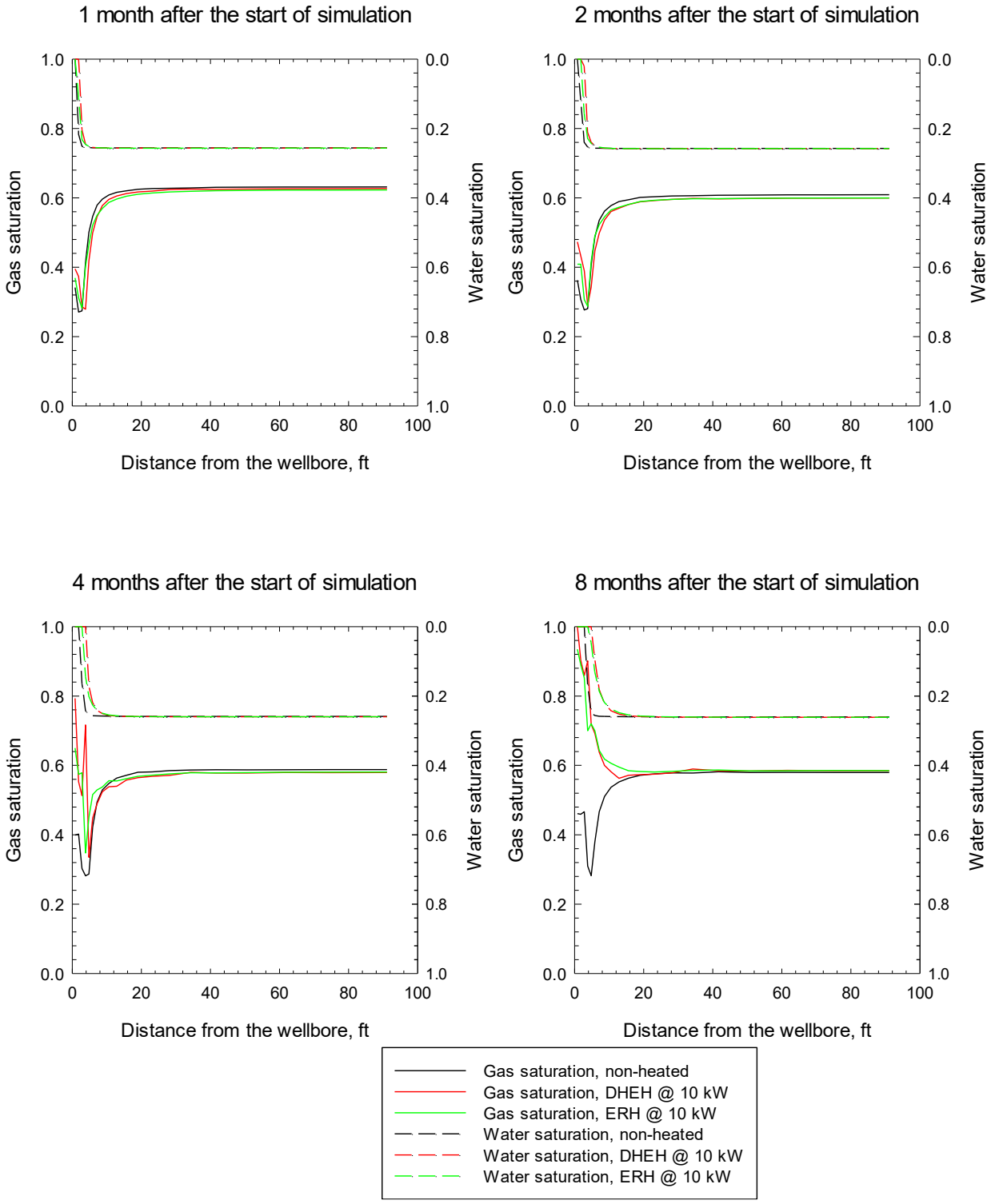

Figure 31. The gas and water saturation profile of the fifth layer in the 0.1 mD reservoir at 1, 2, 4, and 8 months after the start of the simulation.

4.3 NPV Analysis

By making assumptions summarized in **Table 7**, the NPV of the DHEH and ERH operations can be calculated from the above simulation results. **Table 8** summarizes the cash flow and NPV of the two heating methods with different powers in the 0.01 mD reservoir. The cash flow and NPV of the operations in the reservoirs of two other permeabilities are also calculated, but they are not shown and analyzed here because the high-permeability reservoirs deplete much more rapidly than the low-permeability reservoirs. As seen from Table 8, some NPVs decrease in the third year of operation. This suggests that the operation can be terminated earlier for maximizing profitability. NPVs of all heating schemes in the 0.01 md reservoir are positive in some period of the operation, proving their economic feasibility under the assumptions made in this study.

Table 7. Assumptions used to calculate the NPV of the operations.

Parameters	Assumption	Comments
Initial Investment for DHEH	$ 25,000	Heater installed during completion
Initial Investment for ERH	$ 30,000	Electrode installed during completion
Annual Operating Cost	$ 2,000	Excluding the cost of electricity
Annual Discount Rate	10%	
Gas Price	2.03 $/MMBtu	2020 Henry Hub Natural gas average closing price[a]
Oil Price	39.16 $/bbl	2020 WTI average closing price[a]
Electricity price	0.058 $/kWh	
Residual value	$ 0	The downhole assembly cannot be recovered once installed.

a: U.S. Energy Information Administration

It can be seen from Table 8 that the DHEH method with 5 kW of heating power has the highest NPV at the end of the third year. However, the DHEH with 10 kW of heating power has an even

higher NPV at the end of the second year. Since the modelled conceptual reservoir is relatively small, and the economical estimation is conservative, the NPV is expected to be even better in a reservoir of a larger scale.

Table 8. NPV and cash flow of the ERH and DHEH operations in the 0.01 mD reservoir.

		Year 0	Year 1	Year 2	Year 3
ERH @ 5 kW	Cash flow ($)	-30,000.00	15,430.64	23,494.20	4,709.10
	NPV ($)	-30,000.00	-15,972.15	3,444.55	6,982.57
ERH @ 10 kW	Cash flow ($)	-30,000.00	43,884.48	8,750.71	-6,354.74
	NPV ($)	-30,000.00	9,894.98	17,126.98	12,352.57
ERH @ 20 kW	Cash flow ($)	-30,000.00	46,974.42	1,408.93	-12,996.21
	NPV ($)	-30,000.00	12,704.01	13,868.42	4,104.17
DHEH @ 5 kW	Cash flow ($)	-25,000.00	34,641.83	13,014.95	-1,531.87
	NPV ($)	-25,000.00	6,492.57	17,248.73	16,097.81
DHEH @ 10 kW	Cash flow ($)	-25,000.00	43,069.59	7,910.27	-6,972.75
	NPV ($)	-25,000.00	14,154.17	20,691.58	15,452.85
DHEH @ 20 kW	Cash flow ($)	-25,000.00	47,357.11	-2,215.46	-13,699.83
	NPV ($)	-25,000.00	18,051.92	16,220.96	5,928.07

4.4 EROI

We assume that the overall power generation and supply efficiency that takes the power plant efficiency, line losses, transformer losses, etc., into account is 30%. We also assume that the calorific value of the produced gas is 1235 Btu/SCF, and that of the produced oil is 5.8 MMBtu/STB. We ignore any other energy consumption such as the energy involved in the installation of equipment. Based on these assumptions, the EROI of the 0.01 mD permeability model with different heating powers and different heating methods over the three-year simulation period can be then estimated. The detailed data are summarized in **Table 9**. The EROI decreases

as the heating power rises for both methods. The DHEH with 5 kW of power model has the highest EROI of 14.23.

Table 9. EROI of ERH and DHEH with different power in the 0.01 mD horizontal permeability reservoir.

Heating method and power	EROI
ERH @ 5 kW	13.15
ERH @ 10 kW	7.82
ERH @ 20 kW	4.08
DHEH @ 5 kW	14.23
DHEH @ 10 kW	7.66
DHEH @ 20 kW	3.85

Therefore, for both heating approaches, the energy efficiency is higher when they are operated with a lower power. Although the estimation is rough, it is safe to claim that the heating remedial methods, after being optimized according to the geological conditions, will yield better energy efficiency compared with the other unconventional hydrocarbon resources (such as shale oil or bitumen).

References

U.S. Energy Information Administration. (2021). Cushing, OK WTI Spot Price FOB.

U.S. Energy Information Administration. (2021). Henry Hub Natural Gas Spot Price.

Chapter 5 Conclusions & Recommendations

5.1 Conclusions

This study provides alternative remedial solutions for gas condensate wells suffering from condensate blockage. The heating methods studied in this work show generally better performance than the conventional gas injection method. Both of the two heating approaches are suitable for formations with a lower permeability such as shale and tight sandstones. Heating the near-wellbore region with a downhole electrical heater or electrical resistance heating significantly relieves the severe damage caused by condensate blockage in tight formations, restoring the economic recovery of both condensate and gas. Different reservoir conditions and heating scenarios are simulated, leading to the following conclusions:

1) The injection of CH_4 or CO_2 seems to have a better production remediation effect than the injection of pure N_2. However, injecting CO_2-N_2 or CH_4-N_2 mixtures may yield acceptable performance with reduced cost.
2) The ERH and DHEH heating methods show similar performance. At a high heating power, the ERH method yields slightly better performance than the DHEH heating method. Both methods perform better than the gas injection method.
3) The new heating-based method performs better in low-permeability formations. With the same heating power, a low-permeability formation shall be more appropriate for condensate removal treatments, resulting in a more obvious production boost.
4) The ERH method generates a greater heat penetration depth than the DHEH method under the same heating power.

5) The NPV analysis shows that a good economical profitability on both heating methods can be achieved under most of the simulated circumstances. However, in real-world applications, the most profitable operating power should be optimized according to the actual reservoir conditions. It is anticipated that an even better economical profitability can be achieved in a larger reservoir setting.
6) Among all the simulation cases, the DHEH approach with an operating power of 5 kW leads to the highest EROI of 14.23 in the 0.01 mD reservoir. Both heating approaches show better energy efficiency under lower heating power settings.

5.2 Recommendations

In this study, the simulations have been run on a relatively simple conceptual reservoir model. A more realistic reservoir model needs to be built and studied in future works. The reservoir model should be an actual geological model that is built based on the collected data pertinent to cores, well logging, and well testing, etc. In addition, since many low-permeability shale or tight reservoirs are naturally fractured, a dual-porosity model should be adopted to better capture the fluid flow mechanisms in such reservoirs that are subjected to heating treatments. The application of such methods in hydraulically fractured reservoirs could be also studied.

It is worth trying to implement the other heating approaches such as high-frequency electromagnetic heating. In addition, more operational schemes, such as unevenly distributed heating for heterogeneous reservoirs and time-varying heating power, would be considered in the numerical simulations. If proven effective, these schemes may help expand the applicable scope and further bring down the operational cost. Finally, laboratory tests and pilot field tests can be conducted to validate the findings revealed from our numerical simulations.

Bibliography

Alafnan, S., Aljawad, M., Alismail, F., & Almajed, A. (2019). Enhanced Recovery from Gas Condensate Reservoirs through Renewable Energy Sources. Energy and Fuels, 33(10), 10115–10122.

Al-Anazi, H. A., Pope, G. A., Sharma, M. M., & Metcalfe, R. S. (2002). Laboratory Measurements of Condensate Blocking and Treatment for Both Low and High Permeability Rocks. SPE 77546.

Atlason, R., & Unnthorsson, R. (2014). Ideal EROI (Energy Return on Investment) Deepens the Understanding of Energy Systems. Energy, 67, 241–245.

Aziz, R. M. (1983). A 1982 Critique on Gas Cycling Operations on Gas-Condensate Reservoirs. SPE 11477.

Cleveland, C. J., & O'Connor, P. A. (2011). Energy Return on Investment (EROI) of Oil Shale. Sustainability, 3(11), 2307–2322.

Cluff, R. M., & Byrnes, A. P. (2010). Relative Permeability in Tight Gas Sandstone Reservoirs - the "Permeability Jail" Model. SPWLA-2010-58470.

CMG Ltd. (2017). CMG STARS User Guide.

Du, L., Walker, J. G., Pope, G. A., Sharma, M. M., & Wang, P. (2000). Use of Solvents to Improve the Productivity of Gas Condensate Wells. SPE 62935.

Fong, D.K.S., & Nghiem, L.X. (1980). A Viscosity Model for Reservoir Fluids. Computer Modelling Group Research Report R7.02.

Fulcher Jr., R. A., Ertekin, T., & Stahl, C. D. (1985). Effect of Capillary Number and Its Constituents on Two-Phase Relative Permeability Curves. Journal of Petroleum Technology, 37(02), 249–260.

Guo, H., Wang, F., Li, Y., Yu, Z., Gao, X., Gu, Y., Chen, J., Feng, S., & Zhang, X. (2015). Progress on Flow Mechanism in Low Permeability Formation. Procedia Engineering, 126, 466–470.

Hall, C. A. S., Lambert, J. G., & Balogh, S. B. (2014). EROI of Different Fuels and The Implications for Society. Energy Policy, 64, 141–152.

Hinchman, S. B., & Barree, R. D. (1985). Productivity Loss in Gas Condensate Reservoirs. SPE 14203.

Hong, K. C., & Hsueh, L. (1987). Comparison of K-Value Calculation Methods in Compositional Steamflood Simulation. SPE Reservoir Engineering, 2(02), 249–257.

Khan, M. Y., & Jain, P. K. (1999). Theory and Problems in Financial Management. Tata McGraw-Hill Education.

Kuenen, J. P. (1892). On Retrograde Condensation and the Critical Phenomena of Two Substances. Communications from the Physical Laboratory of the University of Leiden.

Kumar, V., Pope, G. A., & Sharma, M. M. (2006). Improving the Gas and Condensate Relative Permeability Using Chemical Treatments. SPE 100529.

Lee, B.I., & Kesler, M.G. (1975). A Generalized Thermodynamic Correlation Based on Three-Parameter Corresponding States. AIChE Journal, 21(3), 510–527.

Li, R. Chen, Z., Wu, K., Liu, X., Dou, L. Yang, S., & Xu, J. (2020). A Fractal Model for Gas-Water Relative Permeability Curve in Shale Rocks. Journal of Natural Gas Science and Engineering, 81, 103417.

Moghaddam, R. N., & Jamiolahmady, M. (2019). Steady-State Relative Permeability Measurements of Tight and Shale Rocks Considering Capillary End Effect. Transport in Porous Media, 128, 75–96.

Murphy, D., & Hall, C. (2010). Year in Review-EROI Or Energy Return On (Energy) Invested. Annals of the New York Academy of Sciences, 1185, 102–118.

Orangi, A., Nagarajan, N. R., Honarpour, M. M., & Rosenzweig, J. (2011). Unconventional Shale Oil and Gas-Condensate Reservoir Production, Impact of Rock, Fluid, and Hydraulic Fractures. SPE 140536.

Pedersen, K. S., & Christensen, P. L. (2006). Phase Behavior of Petroleum Reservoir Fluids. CRC Press.

Peng, D.Y., & Robinson, D. B. (1976). A New Two-Constant Equation of State. Industrial & Engineering Chemistry Fundamentals, 15(1), 59–64.

Pope, G., Wu, W., Narayanaswamy, G., Delshad, M., Sharma, M., & Wang, P. (2000). Modeling Relative Permeability Effects in Gas-Condensate Reservoirs with a New Trapping Model. SPE Reservoir Evaluation & Engineering 3 (02), 171–178.

Rahimi, P., Cooper, S., & Alem, T. (2009). Diluent Evaluation for Bitumen Pipelining. The 5. NCUT Upgrading and Refining Conference 2009.

Reid, R.C., Prausnitz, J.M., & Sherwood, T.K. (1977). The Properties of Gases and Liquids, 3rd Edition, McGraw-Hill.

Sayed, M. A., & Al-Muntasheri, G. A. (2016). Mitigation of the Effects of Condensate Banking: A Critical Review. SPE Production and Operations, 31(2), 85–102.

Shanley, K. W., Cluff, R. M., & Robinson, J. W. (2004). Factors Controlling Prolific Gas Production from Low-Permeability Sandstone Reservoirs: Implications for Resource Assessment, Prospect Development, and Risk Analysis. AAPG Bulletin, 88(8), 1083–1121.

U.S. Energy Information Administration. (2021). Cushing, OK WTI Spot Price FOB.

U.S. Energy Information Administration. (2021). Henry Hub Natural Gas Spot Price.

Ward, J. S., & Morrow, N. R. (1987). Capillary Pressures and Gas Relative Permeabilities of Low-Permeability Sandstone. SPE Formation Evaluation, 2(03), 345–356.

Whitson, C. H., & Brulé, M. R., Society of Petroleum Engineers. (2000). Phase Behavior. Henry L. Doherty Memorial Fund of AIME, Society of Petroleum Engineers.

Whitson, C. H., & Torp, S. B. (1983). Evaluating Constant-Volume Depletion Data. Journal of Petroleum Technology, 35(03), 610–620.

Appendix

Relative Permeability Model Based on Trapping Number

The trapping number (N_T) is defined as the vector sum of the capillary number (N_C) and the Bond number (N_B) (Pope et al., 2000):

$$N_{T_l} = N_{C_l} + N_{B_l} = \frac{\left|\vec{\vec{k}} \cdot \left(\vec{\nabla}\phi_{l'} + g(\rho_{l'} - \rho_l)\vec{\nabla}D\right)\right|}{\sigma_{ll'}} \quad \textbf{(A1.1)}$$

where $\vec{\vec{k}}$ is the permeability tensor; $\vec{\nabla}\phi$ is the flow potential gradient; g is the gravitational constant; ρ is the density; D is the depth; and σ is the interfacial tension. The subscript l denotes one phase (usually the trapped phase), and the subscript l' denotes the conjugate phase (usually the displacing phase).

The model firstly develops a relationship between the residual saturation and the trapping number of each phase (Pope et al., 2000)

$$S_{lr} = min\left(S_l, S_{lr}^{high} + \frac{S_{lr}^{low} - S_{lr}^{high}}{1 + T_l\left(N_{T_l}\right)^{\tau_l}}\right) \quad \text{(A1.2)}$$

where S_l is the saturation of phase l, and S_{lr} is the residual saturation of phase l. The superscripts *high* and *low* represent the conditions at high or low trapping number, respectively. T_l and τ_l are two parameters obtained by data fitting.

Next, the model correlates the endpoint permeability of each phase by the following equation (Pope et al., 2000)

$$k_{rl}^{0} = k_{rl}^{0\,low} + \frac{S_{lr}^{low} - S_{lr}}{S_{lr}^{low} - S_{lr}^{high}}\left(k_{rl}^{0\,high} - k_{rl}^{0\,low}\right) \tag{A1.3}$$

where k_{rl} is the relative permeability of phase l, and k_{rl}^{o} is the endpoint relative permeabilty of phase l.

Finally, the model calculates the relative permeability of each phase as a function of saturation by the following equation (Pope et al., 2000):

$$\log k_{rl} = \log k_{rl}^{0} + \log \overline{S_l} + \frac{log\left(\frac{k_{rl}}{k_{rl}^{0}}\right)^{low} - log\,\overline{S_l}}{1 + T_{l'}\left(N_{T_l}\right)^{\tau_{l'}}} \tag{A1.4}$$

in which $\overline{S_l}$ is the normalized saturation of phase l, and can be calculated as (Pope et al., 2000):

$$\overline{S_l} = \frac{S_l - S_{lr}}{1 - \sum_{l=1}^{n_p} S_{lr}} \tag{A1.5}$$